

Probabilistic Joint and Individual Variation Explained (ProJIVE) for Data Integration

Raphael J. Murden¹, Ganzhong Tian¹, Deqiang Qiu², Benjamin B. Risk^{*1},
and FOR THE ALZHEIMER'S DISEASE NEUROIMAGING
INITIATIVE^{†3}

¹Department of Biostatistics and Bioinformatics, Rollins School of Public Health, Emory University, 1518 Clifton Rd NE, Atlanta, GA 30322, USA

²Department of Radiology and Imaging Sciences, Emory University School of Medicine, 1364 Clifton Rd NE, Atlanta, GA 30322, USA

x

Abstract

Collecting multiple types of data on the same set of subjects is common in modern scientific applications including genomics, metabolomics, and neuroimaging. Joint and Individual Variation Explained (JIVE) seeks a low-rank approximation of the joint variation between two or more sets of features captured on common subjects and isolates this variation from that unique to each set of features. We develop an expectation-maximization (EM) algorithm to estimate a probabilistic model for the JIVE framework. The model extends probabilistic PCA to multiple datasets. Our maximum likelihood approach simultaneously estimates joint and individual components, which can lead to greater accuracy compared to other methods. We apply ProJIVE to measures of brain morphometry and cognition in Alzheimer's disease. ProJIVE learns biologically meaningful sources of variation, and the joint morphometry and cognition subject scores are strongly related to more expensive existing biomarkers. Data used in preparation of this article were obtained from the Alzheimer's Disease Neuroimaging Initiative (ADNI) database. Code to reproduce the analysis is available at <https://github.com/thebrisklab/ProJIVE>. Supplementary materials for this article are available online.

*brisk@emory.edu, 1518 Clifton Rd NE, Atlanta, GA 30322

[†]Data used in preparation of this article were obtained from the Alzheimer's Disease Neuroimaging Initiative (ADNI) database (adni.loni.usc.edu).

Keywords: ADNI; Alzheimer's Disease; JIVE; Multi-block data analysis; Multimodal data analysis; Neuroimaging statistics; Probabilistic PCA

1 Introduction

Data integration methods analyze multiple datasets collected from the same participants. Collections of datasets have become common in neuroimaging, genomics, proteomics, and other fields (Mueller et al., 2005; Allen et al., 2014; Tomczak et al., 2015). Statistical approaches to data integration date as far back as the 1930s, with the introduction of Canonical Correlation Analysis (CCA) (Hotelling, 1936). While CCA focuses on exploring structure that is shared (i.e., joint) between two datasets, more recently, methods such as JIVE (Joint and Individual Variance Explained) add to the data integration framework by also extracting structure that is unique (i.e., individual) to each of the datasets (Lock et al., 2013).

The current manuscript develops a probabilistic, model-based method to implement JIVE. Several data integration methods related to JIVE have been developed in recent years. R.JIVE iterates between estimating the joint matrices and individual matrices until convergence, and it was used to explore the relationship between microRNA and gene expression in patients with malignant brain tumors (Lock et al., 2013; O’Connell and Lock, 2016). AJIVE (Feng et al., 2018) uses matrix perturbation theory to estimate joint ranks and a non-iterative method for extracting joint structure, followed by a separate step to estimate individual structure. This approach was applied to behavioral and imaging data from the Human Connectome Project (Yu et al., 2017). Bayesian Simultaneous Factorization and Prediction uses a Bayesian probabilistic model for a JIVE decomposition of multi-omic predictors to predict an outcome (Samorodnitsky et al., 2024). Other data integration methods include the following: robust-JIVE, which utilizes an L-1 norm minimization technique for computer vision applications (Sagonas et al., 2017); Common and Orthogonal Basis Extraction, which is similar to JIVE (Zhou et al., 2016); Structural Learning and Integrative Decomposition, which allows for partially shared structure (Gaynanova and Li, 2019); Data Integration Via Analysis of Subspaces (DIVAS), which estimates partially shared structure

using principal angles between subspaces and uses a rotational bootstrap to estimate the signal ranks (Prothero et al., 2024); Decomposition-based Canonical Correlation Analysis (D-CCA), a CCA method that includes individual random variables with covariance equal to zero (Shu et al., 2020); Simultaneous Non-Gaussian Component Analysis, which uses non-Gaussianity for dimension reduction rather than variance (Risk and Gaynanova, 2021); and Generalized Integrative Principal Component Analysis (GIPCA), which extends principal component analysis for exponential family densities to data integration (Zhu et al., 2020).

While much progress has been made in data integration studies, many of the previous methods do not propose statistical models. For instance, JIVE was formulated as a framework for decomposing data into matrices defined by score subspaces, and a generative model for a new subject was not defined. We will argue that a data integration method using maximum likelihood to model subject scores and loadings may improve both accuracy and interpretability. Unlike JIVE, Bayesian Simultaneous Factorization and Prediction, D-CCA, and GIPCA propose statistical models with latent variables. Bayesian simultaneous factorization and prediction involves priors and hyperparameters in a Bayesian framework, which may be computationally challenging. D-CCA is only formulated for two datasets and involves multiple estimation steps. GIPCA uses the single parameter exponential family without dispersion (variance) parameters, which we will examine in simulations.

Probabilistic principal component analysis, or pPCA, formulates a statistical model for PCA in which subject scores are normally distributed random effects and variable loadings are fixed parameters (Bishop, 1999). The pPCA model is a special case of the factor analysis model (Lawley and Maxwell, 1962), where the former assumes the errors have a diagonal covariance matrix with equal variances, and the latter assumes a diagonal covariance matrix in which variances can differ. We generalize the pPCA framework to two or more datasets and develop a probabilistic approach to JIVE, which we call Probabilistic JIVE or ProJIVE.

ProJIVE models sources of joint variation as subject random effects shared between datasets and sources of individual variation as subject random effects unique to each dataset. Our approach increases interpretability by directly modeling quantities of interest, may be more accurate than a multi-step decomposition process, and can be useful when the covariance matrix is a useful summary measure, including some applications in which data are not Gaussian.

Our model is closely related to inter-battery factor analysis (IBFA) (Tucker, 1958). Our contributions include a latent variable model and novel algorithm. IBFA posits latent variables shared by two datasets and latent variables unique to each dataset and, therefore, is closely related to JIVE. Early work derived a maximum likelihood solution for Gaussian-distributed joint scores but did not assume a low-rank structure for the unique factors (Browne, 1979). More recently, Klami et al. (2013) proposed a Bayesian inter-battery factory analysis for two datasets and Klami et al. (2014) proposed group factor analysis for multiple datasets, which use variational inference to approximate the likelihoods and sparsity priors to approximate block-wise sparsity.

In Section 2, we describe the ProJIVE model, identifiability, and an EM algorithm to estimate its parameters. Section 3 conducts a simulation study comparing ProJIVE to existing JIVE methods. ProJIVE achieved greater accuracy in estimating scores and variable loadings when compared to R.JIVE, AJIVE, and GIPCA in a variety of simulation settings, including non-Gaussian simulations. In Section 4, we evaluate the effectiveness of ProJIVE via an analysis of data obtained from the Alzheimer’s Disease Neuroimaging Initiative (ADNI). Our application to the ADNI data integrates measures of brain morphometry (i.e., thickness, surface area, and volume) with measures of cognition and behavior to estimate their joint sources of variation. Results demonstrate ProJIVE’s utility: joint subject scores strongly associate with variables such as AD diagnosis, the presence of the genetic marker apolipopro-

tein E4 (ApoE4), amyloid-beta levels from Positron Emission Tomography (PET) imaging using florbetapir (18F-AV45), and neuronal cell metabolism derived from fluorodeoxyglucose (FDG) PET. Section 5 discusses our model and limitations. Proofs are in the Supporting Information.

2 Methods

2.1 The original JIVE decomposition

Suppose features arising from the same set of n observational units (e.g., subjects) are collected in different datasets, \mathbf{X}_k for $k = 1, \dots, K$, such that each dataset has dimension $p_k \times n$. JIVE assumes $\mathbf{X}_k = \mathbf{J}_k + \mathbf{A}_k + \mathbf{E}_k$, where \mathbf{J}_k is the joint signal, \mathbf{A}_k the individual signal, and \mathbf{E}_k the noise, where $\mathbb{E}(\mathbf{E}_k) = \mathbf{0}$ with mutually independent entries. Let $\text{Row}(\mathbf{G})$ define the row space of a matrix \mathbf{G} : $\text{Row}(\mathbf{G}) = \{\mathbf{v} \in \mathbb{R}^n : \mathbf{v}^\top = \mathbf{t}^\top \mathbf{G} \text{ for some } \mathbf{t} \in \mathbb{R}^{p_k}\}$. The JIVE framework assumes (i) $\text{Row}(\mathbf{J}_k) = \text{Row}(\mathbf{J}_{k'})$ for $k \neq k' \in \{1, \dots, K\}$; (ii) $\text{Row}(\mathbf{J}_k) \perp \text{Row}(\mathbf{A}_k)$ (i.e., $\mathbf{J}_k \mathbf{A}_k^\top = \mathbf{0}$); and (iii) $\bigcap_{k=1, \dots, K} \text{Row}(\mathbf{A}_k) = \mathbf{0}$ (Lock et al., 2013; Feng et al., 2018). R.JIVE includes a variant in which $\text{Row}(\mathbf{A}_k) \perp \text{Row}(\mathbf{A}_{k'})$, $k = 1, \dots, K$ (O’Connell and Lock, 2016). The decomposition $\mathbf{X}_k = \mathbf{J}_k + \mathbf{A}_k + \mathbf{E}_k$ is unique when one assumes $\text{rank}(\mathbf{J}_k) + \text{rank}(\mathbf{A}_k) = \text{rank}(\mathbf{J}_k + \mathbf{A}_k)$, $k = 1, \dots, K$ (Lock et al., 2013). Feng et al. (2018) further assume that the noise is isotropic.

2.2 Probabilistic JIVE

We propose a probabilistic model for $\mathbf{x}_{ik} \in \mathbb{R}^{p_k}$, which represents the random vector of p_k features from the i th subject, $i = 1, \dots, n$, in the k th data block, $k = 1, \dots, K$. Assume $\mathbb{E}(\mathbf{x}_{ik}) = \mathbf{0}$. Let r_J define the number of joint components and r_{Ik} the number of individual components in the k th dataset. The loading matrices $\mathbf{W}_{Jk} \in \mathbb{R}^{p_k \times r_J}$ and $\mathbf{W}_{Ik} \in \mathbb{R}^{p_k \times r_{Ik}}$

represent variable-specific summaries to joint and individual variance, respectively, for the k^{th} data-block. Our model is given by

$$\mathbf{x}_{ik} = \mathbf{W}_{Jk}\mathbf{z}_i + \mathbf{W}_{Ik}\mathbf{b}_{ik} + \boldsymbol{\epsilon}_{ik}, \quad (1)$$

$$(\mathbf{z}_i^\top, \mathbf{b}_{i1}^\top, \dots, \mathbf{b}_{iK}^\top)^\top \stackrel{iid}{\sim} N(\mathbf{0}, \mathbf{I}), \quad \boldsymbol{\epsilon}_{ik} \stackrel{iid}{\sim} N(\mathbf{0}, \mathbf{D}_k), \quad \text{Cov}(\boldsymbol{\epsilon}_{ik}, \boldsymbol{\epsilon}_{ik'}) = \mathbf{0},$$

$$\text{Cov}[(\mathbf{z}_i^\top, \mathbf{b}_{i1}^\top, \dots, \mathbf{b}_{iK}^\top)^\top, \boldsymbol{\epsilon}_{ik}] = \mathbf{0},$$

$$\text{rank}(\mathbf{W}_{Jk}) = r_J, \quad \text{rank}([\mathbf{W}_{Jk}, \mathbf{W}_{Ik}]) < p_k, \quad \text{and } \{k, k'\} \subseteq 1, \dots, K, \quad \text{where } \mathbf{D}_k \text{ is diagonal.}$$

In our identifiability results in Section 2.4, we further assume that $\mathbf{D}_k = \sigma_k^2 \mathbf{I}$. Then under this block-specific isotropic error assumption, the model can be seen as an extension of probabilistic PCA (Tipping and Bishop, 1999) to multiple datasets, where the joint scores \mathbf{z}_i capture shared information.

In our application (Section 4), we center the data such that $\sum_i \mathbf{x}_{ik} = \mathbf{0}$ and we normalize each variable to unit variance. We recommend normalization when the variables within each data block are measured in different units or scales, as in the cognitive dataset, or when variables should be weighed equally, as desired for the brain regions in our neuroimaging dataset. However, variance normalization may be inappropriate in bulk sample gene expression, where normalization could result in a large biological signal being downweighted relative to genes with no signal but comparable measurement error.

In many applications, joint scores are of particular interest and can be investigated as potential prodromes or discriminating factors among subgroups (Lock et al., 2013). On the other hand, examination of the joint and individual variable loadings $\{\mathbf{W}_{Jk}, \mathbf{W}_{Ik} : k = 1, \dots, K\}$ can lead to discovery of the features that drive shared variation or individual variation (Yu et al., 2017; Kashyap et al., 2019).

For the case of $K = 2$, the covariance of the ProJIVE model is

$$\text{Cov} \begin{pmatrix} \mathbf{x}_{i1} \\ \mathbf{x}_{i2} \end{pmatrix} = \begin{pmatrix} \mathbf{W}_{J1}\mathbf{W}_{J1}^\top + \mathbf{W}_{I1}\mathbf{W}_{I1}^\top + \mathbf{D}_1 & \mathbf{W}_{J1}\mathbf{W}_{J2}^\top \\ \mathbf{W}_{J2}\mathbf{W}_{J1}^\top & \mathbf{W}_{J2}\mathbf{W}_{J2}^\top + \mathbf{W}_{I2}\mathbf{W}_{I2}^\top + \mathbf{D}_2 \end{pmatrix}. \quad (2)$$

Let $\mathbf{x}_i = [\mathbf{x}_{i1}^\top, \dots, \mathbf{x}_{iK}^\top]^\top$, $i = 1, \dots, n$, and recall that we assume $\mathbb{E} \mathbf{x}_i = 0$. Define the population covariance matrix: $\mathbf{C} = \text{Cov}(\mathbf{x}_i)$. The log-likelihood is

$$\ell(\mathbf{W}_{Jk}, \mathbf{W}_{Ik}, \mathbf{D}_k, k = 1, \dots, K; \mathbf{x}_1, \dots, \mathbf{x}_n) = -\frac{n}{2} \{\log(|2\pi\mathbf{C}|) + \text{tr}(\mathbf{C}^{-1}\mathbf{S})\}, \quad (3)$$

where $\mathbf{S} = \frac{1}{n} \sum_{i=1}^n \mathbf{x}_i \mathbf{x}_i^\top$, $|\cdot|$ denotes the determinant, and $\text{tr}(\cdot)$, the trace.

2.3 Connections between ProJIVE and previous models

We discuss three orthogonality assumptions and their relationship to other data integration methods. (i) *Orthogonality between joint and individual scores.* We assume $\text{Cov}(\mathbf{z}_i, \mathbf{b}_{ik}) = 0$, which is the random variable analogue of the orthogonality between joint and individual subspaces that is assumed in JIVE (Lock et al., 2013; Feng et al., 2018). Rather than enforce orthogonality of the matrices with respect to the Euclidean inner product (which is done in JIVE), we will use a Gaussian likelihood with the EM algorithm to achieve our decomposition. (ii) *Orthogonality between individual scores.* We further assume $\text{Cov}(\mathbf{b}_{ik}, \mathbf{b}_{ik'}) = 0$, and in this respect is similar to the assumption of orthogonality on the \mathcal{L} -2 space of random variables in D-CCA (D-CCA is defined for the special case of $K = 2$, does not assume Gaussianity, and does not assume orthogonality between joint and individual) (Shu et al., 2020). (iii) *Mutual orthogonality:* $\text{Cov}(\mathbf{z}_i, \mathbf{b}_{ik}) = 0$ and $\text{Cov}(\mathbf{b}_{ik}, \mathbf{b}_{ik'}) = 0$. This contrasts with AJIVE and D-CCA, but mutual orthogonality conditions were considered in R.JIVE, where it increased robustness to mis-specified ranks (O’Connell and Lock, 2016). Mutual

orthogonality was also enforced in [Gaynanova and Li \(2019\)](#), who developed the model for partially shared structure.

Although beyond the scope of this paper, our approach naturally extends to the partially shared structure considered in [Gaynanova and Li \(2019\)](#). We can define random variables that are only shared between some of the datasets. For $K = 3$, we could augment the model to include partially shared latent factors, e.g., $\mathbf{z}_{i,12}$ shared between datasets 1 and 2 and $\mathbf{z}_{i,13}$ shared between datasets 1 and 3,

$$\mathbf{x}_{i1} = \mathbf{W}_{J1}\mathbf{z}_i + \mathbf{W}_{P(1,2),1}\mathbf{z}_{i,12} + \mathbf{W}_{P(1,3),1}\mathbf{z}_{i,13} + \mathbf{W}_{I1}\mathbf{b}_{i1} + \boldsymbol{\epsilon}_{i1}, \quad (4)$$

where $\mathbf{W}_{P(1,2),1}$ and $\mathbf{W}_{P(1,3),1}$ capture the loadings on dataset 1 for the partially shared structure between datasets 1 and 2 and datasets 1 and 3, respectively.

2.4 Model identifiability

It is easy to see that the density defined by (1) is invariant to orthogonal transformations of the components. For the general case in which we allow for diagonal \mathbf{D}_k , identifiability results are challenging. The situation is the same as occurs in factor analysis, in which there exist cases where the signal and noise are not uniquely identified ([Shapiro, 1985](#)). In this section, we examine the case with $\mathbf{D}_k = \sigma_k^2\mathbf{I}$ for $k = 1, 2$. Isotropic errors were also assumed in AJIVE ([Feng et al., 2018](#)) Interestingly, the joint scores and loadings have an indeterminacy up to certain linear transformations that form a set larger than the set of orthogonal transformations. Let $\mathbf{A} \succeq 0$ denote that a matrix \mathbf{A} is positive semidefinite. Let \mathcal{O} denote the class of orthogonal matrices.

Theorem 1. *Suppose $K = 2$ and let f_{Φ} define the multivariate normal density according to the parameters $\{\mathbf{W}_{J1}, \mathbf{W}_{J2}, \mathbf{W}_{I1}, \mathbf{W}_{I2}, \sigma_1^2, \sigma_2^2\}$ and the assumptions in (1). Let f_{Φ^*} denote*

the multivariate normal density with parameters $\{\mathbf{W}_{J_1}^*, \mathbf{W}_{J_2}^*, \mathbf{W}_{I_1}^*, \mathbf{W}_{I_2}^*, \sigma_1^{*2}, \sigma_2^{*2}\}$ and the assumptions in (1). Then $f_\Phi = f_{\Phi^*}$ if and only if

1. $\sigma_1^{*2} = \sigma_1^2, \sigma_2^{*2} = \sigma_2^2,$

2. There exists an $r_J \times r_J$ non-singular matrix \mathbf{T}_1 such that $\mathbf{W}_{J_1}^* = \mathbf{W}_{J_1} \mathbf{T}_1$ and $\mathbf{W}_{J_2}^* = \mathbf{W}_{J_2} (\mathbf{T}_1^{-1})^\top$ and

$$\mathbf{W}_{I_1} \mathbf{W}_{I_1}^\top + \mathbf{W}_{J_1} (\mathbf{I} - \mathbf{T}_1 \mathbf{T}_1^\top) \mathbf{W}_{J_1}^\top \succeq 0, \quad (5)$$

$$\mathbf{W}_{I_2} \mathbf{W}_{I_2}^\top + \mathbf{W}_{J_2} (\mathbf{I} - (\mathbf{T}_1^{-1})^\top \mathbf{T}_1^{-1}) \mathbf{W}_{J_2}^\top \succeq 0, \quad (6)$$

3. $\mathbf{W}_{I_1}^*$ is defined such that $\mathbf{W}_{I_1}^* (\mathbf{W}_{I_1}^*)^\top = \mathbf{W}_{I_1} \mathbf{W}_{I_1}^\top + \mathbf{W}_{J_1} (\mathbf{I} - \mathbf{T}_1 \mathbf{T}_1^\top) \mathbf{W}_{J_1}^\top$, and $\mathbf{W}_{I_2}^*$ is defined such that $\mathbf{W}_{I_2}^* (\mathbf{W}_{I_2}^*)^\top = \mathbf{W}_{I_2} \mathbf{W}_{I_2}^\top + \mathbf{W}_{J_2} (\mathbf{I} - (\mathbf{T}_1^{-1})^\top \mathbf{T}_1^{-1}) \mathbf{W}_{J_2}^\top$.

The proof is in Web Appendix A. In short, this theorem provides the necessary and sufficient conditions for different parameters to obtain the same likelihood. Item 1 indicates the error variances are identifiable. Item 2 indicates the joint loadings are identifiable up to a class of linear transformations that includes all orthogonal matrices and possibly some nonsingular matrices. The number of joint components is identifiable, since $\text{Cov}(\mathbf{x}_{i1}, \mathbf{x}_{i2})$ has to have rank r_J . Item 3 indicates that when a non-orthogonal \mathbf{T}_1 exists satisfying (5) and (6), the individual loading matrices are susceptible to leakage from the joint signal. In this case, the number of individual components may also not be identifiable. We provide an example of this with our supplementary code available at <https://github.com/thebrisklab/ProJIVE>. Define the joint variation as $R_{Jk}^2 = \|\mathbf{W}_{Jk}\|_F^2 / \sum_{j=1}^{p_k} \text{var}(x_{ijk})$, where $\text{var}(x_{ijk})$ is the variance of the j th variable in the k th dataset. When a non-orthogonal \mathbf{T}_1 exists satisfying (5) and (6), the breakdown of the joint versus individual variation is not identifiable.

It is interesting to consider the case in which the columns of \mathbf{W}_{Jk} and \mathbf{W}_{Ik} are not linearly independent, i.e., $\text{Col}(\mathbf{W}_{Jk}) \cap \text{Col}(\mathbf{W}_{Ik}) \neq \{\mathbf{0}\}$. Then there can exist \mathbf{T}_k not in

\mathcal{O} that satisfy (5) and (6). Linearly dependent columns between \mathbf{W}_{Jk} and \mathbf{W}_{Ik} occur by construction in the D-CCA decomposition, see equation (16) in [Shu et al. \(2020\)](#). Insight can be gained by examining the case of $\mathbf{W}_{J1} = \mathbf{W}_{I1}$, $\mathbf{W}_{J2} = \mathbf{W}_{I2}$, and $\mathbf{T}_1 = \lambda \mathbf{I}$. Then from (5) and (6), we have $(2 - \lambda^2)\mathbf{W}_{I1}\mathbf{W}_{I1}^\top \succeq 0$ and $(2 - 1/\lambda^2)\mathbf{W}_{I2}\mathbf{W}_{I2}^\top \succeq 0$, which implies $\frac{1}{2} \leq \lambda^2 \leq 2$. Then defining $\mathbf{W}_{I1}^* = \sqrt{2 - \lambda^2}\mathbf{W}_{I1}$ and $\mathbf{W}_{I2}^* = \sqrt{2 - 1/\lambda^2}\mathbf{W}_{I2}$, we see how the decomposition of joint and individual variation is not unique.

In practice, conventional approaches such as Varimax ([Kaiser, 1959](#)) may be applied to the stacked $[\mathbf{W}_{J1}^\top, \dots, \mathbf{W}_{JK}^\top]^\top$ matrices to improve the interpretability. Another approach is to apply ICA to the stacked loadings to obtain an orthogonal matrix that maximizes their non-Gaussianity similar to multiset CCA + joint ICA ([Sui et al., 2011](#)).

2.5 Expectation-Maximization algorithm for ProJIVE

We now develop an Expectation-Maximization (EM) algorithm to estimate the variable loadings, noise variances, and subject scores.

Consider the latent subject scores, $\{\theta_i = (\mathbf{z}_i^\top, \mathbf{b}_{i1}^\top, \dots, \mathbf{b}_{iK}^\top)^\top : i = 1, \dots, n\}$, as “missing” data, so that the “complete” data include the latent scores and the observed \mathbf{x}_i . Let $\boldsymbol{\epsilon}_i = (\boldsymbol{\epsilon}_{i1}^\top, \dots, \boldsymbol{\epsilon}_{iK}^\top)^\top$ and

$$\mathbf{W} = \begin{pmatrix} \mathbf{W}_{J1} & \mathbf{W}_{I1} & \mathbf{0} & \cdots & \mathbf{0} \\ \vdots & \mathbf{0} & \ddots & \mathbf{0} & \vdots \\ \vdots & \vdots & \mathbf{0} & \ddots & \mathbf{0} \\ \mathbf{W}_{JK} & \mathbf{0} & \cdots & \mathbf{0} & \mathbf{W}_{IK} \end{pmatrix}.$$

Then, equation (1) is equivalent to $\mathbf{x}_i = \mathbf{W}\theta_i + \boldsymbol{\epsilon}_i$.

Let $p = \sum_{k=1}^K p_k$ represent the total number of variables/features in both datasets and $r = r_J + \sum_{k=1}^K r_{Ik}$ the total number of latent components. Let \mathbf{D} be the diagonal matrix

formed with $\mathbf{D}_1, \dots, \mathbf{D}_K$ on the block diagonals. Then, we can write the complete-data log likelihood as

$$\ell_C(\mathbf{W}, \mathbf{D}) = -\frac{n}{2} \{(p+r) \log(2\pi) + \log |\mathbf{D}|\} - \frac{1}{2} \sum_{i=1}^n \{(\mathbf{x}_i - \mathbf{W}\theta_i)^\top \mathbf{D}^{-1} (\mathbf{x}_i - \mathbf{W}\theta_i) + \theta_i^\top \theta_i\}. \quad (7)$$

The definitions of the latent and observed variables lead to a multivariate normal distribution for the complete data vector $(\theta_i^\top, \mathbf{x}_i^\top)^\top \sim N(\mathbf{0}, \Sigma)$ where, $\Sigma = \begin{pmatrix} \mathbf{I}_r & \mathbf{W}^\top \\ \mathbf{W} & \mathbf{C} \end{pmatrix}$.

Define loadings and scores for block k as $\mathbf{W}_k = (\mathbf{W}_{J_k}, \mathbf{W}_{I_k})$ and $\theta_{ik} = (\mathbf{z}_i, \mathbf{b}_{ik})$ and selection matrices $\mathbf{L}_k = (\mathbf{0}_{p_k \times p_1} \dots \mathbf{I}_{p_k \times p_k} \dots \mathbf{0}_{p_k \times p_K})$ and

$$\mathbf{M}_k = \begin{pmatrix} \mathbf{I}_{r_J \times r_J} & \dots & \mathbf{0} & \dots & \mathbf{0} \\ \mathbf{0} & \dots & \mathbf{I}_{r_{I_k} \times r_{I_k}} & \dots & \mathbf{0} \end{pmatrix}.$$

With this parameterization, $\mathbf{x}_{ik} = \mathbf{L}_k \mathbf{x}_i$, $\theta_{ik} = \mathbf{M}_k \theta_i$, and $\mathbf{L}_k \mathbf{W} = \mathbf{W}_k \mathbf{M}_k$. The expectation of the complete log-likelihood, conditioned on the observed data, is

$$\begin{aligned} \mathbb{E}\{\ell_C | \mathbf{x}_i\} &= -\frac{n}{2} \left((p+r) \log(2\pi) + \sum_{k=1}^K \log[\text{tr}(\mathbf{D}_k)] \right) \\ &\quad - \frac{1}{2} \sum_{i=1}^n \sum_{k=1}^K \mathbf{D}_k^{-1} [\mathbf{x}_{ik}^\top \mathbf{x}_{ik} + \text{tr}\{\mathbf{W}_k^\top \mathbf{W}_k \mathbb{E}(\theta_{ik} \theta_{ik}^\top | \mathbf{x}_i)\} - 2\mathbf{x}_{ik}^\top \mathbf{W}_k \mathbb{E}(\theta_{ik} | \mathbf{x}_i)] + \mathbb{E}(\theta_{ik}^\top \theta_{ik} | \mathbf{x}_i). \end{aligned} \quad (8)$$

The first and second conditional moments of the scores for block k take the form

$$\begin{aligned}\mathbb{E}(\theta_{ik}|\mathbf{x}_i) &= \mathbf{M}_k \mathbf{W}^\top \mathbf{C}^{-1} \mathbf{x}_i, \\ \text{Cov}(\theta_{ik}|\mathbf{x}_i) &= \mathbf{M}_k (\mathbf{I}_r - \mathbf{W}^\top \mathbf{C}^{-1} \mathbf{W}) \mathbf{M}_k^\top, \\ \mathbb{E}(\theta_{ik} \theta_{ik}^\top | \mathbf{x}_i) &= \mathbf{M}_k (\mathbf{I}_r - \mathbf{W}^\top \mathbf{C}^{-1} \mathbf{W} + \mathbf{W}^\top \mathbf{C}^{-1} \mathbf{x}_i \mathbf{x}_i^\top \mathbf{C}^{-1} \mathbf{W}) \mathbf{M}_k^\top.\end{aligned}$$

Differentiating the conditional expected log-likelihood with respect to the parameters \mathbf{W}_k and \mathbf{D}_k , then setting each equal to 0 yields closed form solutions given by

$$\begin{aligned}\widetilde{\mathbf{W}}_k &= \left(\sum_i \mathbf{x}_{ik} \mathbb{E}(\theta_{ik}^\top | \mathbf{x}_i) \right) \left(\sum_i \mathbb{E}(\theta_{ik} \theta_{ik}^\top | \mathbf{x}_i) \right)^{-1}, \\ \widetilde{\mathbf{D}}_k &= \text{Diag} \left\{ \frac{1}{n} \sum_i \text{diag} \{ \mathbf{L}_k \mathbf{x}_i \mathbf{x}_i^\top \mathbf{L}_k^\top + \mathbf{W}_k \mathbb{E}(\theta_{ik} \theta_{ik}^\top | \mathbf{x}_i) \mathbf{W}_k^\top - 2 \mathbf{W}_k \mathbb{E}(\theta_{ik} | \mathbf{x}_i) \mathbf{x}_{ik}^\top \} \right\},\end{aligned}\tag{9}$$

where $\text{diag}\{\cdot\}$ extracts the diagonal from a square matrix and $\text{Diag}\{\cdot\}$ constructs a diagonal matrix from the elements of its argument. Assuming $\mathbf{D}_k = \sigma_k^2 \mathbf{I}$, the second equation in (9) becomes $\widetilde{\sigma}_k^2 = \frac{1}{np_k} \sum_i \text{tr} \{ \mathbf{L}_k \mathbf{x}_i \mathbf{x}_i^\top \mathbf{L}_k^\top + \mathbf{W}_k \mathbb{E}(\theta_{ik} \theta_{ik}^\top | \mathbf{x}_i) \mathbf{W}_k^\top - 2 \mathbf{W}_k \mathbb{E}(\theta_{ik} | \mathbf{x}_i) \mathbf{x}_{ik}^\top \}$. We initialize $\mathbf{D}_k = \hat{\sigma}_k^2 \mathbf{I}$, where $\hat{\sigma}_k^2$ is the MLE from the rank $r_J + r_{Ik}$ pPCA of each dataset (average of the smallest $p_k - r_J - r_{Ik}$ eigenvalues for $n > p_k$). We initialized the loading matrices \mathbf{W}_{Jk} and \mathbf{W}_{Ik} using three strategies: (1) the AJIVE solution (Feng et al., 2018); (2) the Cholesky decomposition on the covariance matrix of each dataset, where W_{Jk} is initialized using the first r_J columns and W_{Ik} with the next r_{Ik} columns; (3) standard normal entries. Our code on github provides additional options.

3 Simulation study

3.1 Simulation design

We conducted simulation studies to examine 1) the accuracy of estimates when the joint signal strength (i.e., proportion of variation) is low versus high and 2) robustness against model misspecification. For the centered data matrices such that $\mathbf{X}_k \mathbf{1} = \mathbf{0}$, the proportion of total variation in the k^{th} dataset attributable to the joint signal is $R_{Jk}^2 = \frac{\|\mathbf{J}_k\|_F^2}{\|\mathbf{X}_k\|_F^2}$. The proportion attributable to the individual signal is $R_{Ik}^2 = \frac{\|\mathbf{I}_k\|_F^2}{\|\mathbf{X}_k\|_F^2}$. The individual ranks, sample size, number of features in \mathbf{X}_1 , and proportions of individual variation explained for both data blocks were held constant at $r_{I1} = r_{I2} = 2$, $n = 1000$, $p_1 = 20$, and $R_{J1}^2 = R_{J2}^2 = 0.25$, respectively. We use a full factorial design with the following factors:

1. The joint rank: with levels (a) $r_J = 1$ and (b) $r_J = 3$
2. The number of features in \mathbf{X}_2 : with levels (a) $p_2 = 20$ and (b) $p_2 = 200$,
3. Joint Variation Explained in \mathbf{X}_1 : with levels (a) $R_{J1}^2 = 0.1$ and (b) $R_{J1}^2 = 0.5$,
4. Joint Variation Explained in \mathbf{X}_2 : with levels (a) $R_{J2}^2 = 0.1$ and (b) $R_{J2}^2 = 0.5$,
5. Data generating distributions: with levels (a) Gaussian scores and loadings and (b) mixture of Gaussian joint scores (mixing proportions equal to 0.2, 0.5, and 0.3 with means equal to -4, 0, and 4, respectively, and sd=1 for all three) and Rademacher loadings for both joint and individual components.

We define $\mathbf{W}_{Jk} = \mathbf{R}_{Jk} \mathbf{Q}_J$, $\mathbf{W}_{Ik} = \mathbf{R}_{Ik} \mathbf{Q}_I$ with diagonal matrices $\mathbf{Q}_J = \text{diag}(3, 2, 1)$ and $\mathbf{Q}_I = \text{diag}(2, 1)$ and \mathbf{R}_{Jk} and \mathbf{R}_{Ik} with entries defined by factor five (Gaussian or Rademacher). Entries of the noise matrices \mathbf{E}_1 and \mathbf{E}_2 were randomly drawn from a standard Gaussian distribution. In order to achieve the desired values of R_{Jk}^2 and R_{Ik}^2 , we rescaled

the joint and individual matrices such that $\mathbf{X}_k = d_k \mathbf{J}_K + c_k \mathbf{A}_k + \mathbf{E}_k$ for appropriate constants c_k and d_k , as described in the Web Appendix D.1.

For each combination of settings, we performed 100 simulations using five methods of JIVE analysis: ProJIVE, AJIVE, GIPCA, R.JIVE, and D-CCA, using true signal ranks as input for each. In ProJIVE, the EM algorithm is implemented using the isotropy assumption and initiated using all three strategies discussed in Section 2.5. We evaluated accuracy using the chordal norm, a measure of distance between subspaces (Ye and Lim, 2014), scaled by the rank of the subspace to result in a value contained in $[0, 1]$. The chordal norm is defined in the Web Appendix D.2.

We also conducted a simulation study based on the design from the Feng et al. (2018) example. In this design, observational units in each half of the data block were given joint scores of -1 and 1, respectively. Joint loadings in \mathbf{X}_1 have values 0 for half the variables and 1 for the other half. Joint loadings in \mathbf{X}_2 have values 0 for 80% of the variables and 1 for the remaining 20%. The individual signal for \mathbf{X}_1 comprised one component driven by all variables, which partitioned subjects into two groups. The individual signal for \mathbf{X}_2 comprised two components. The loadings for each individual signal were orthogonal to the joint loadings, and the noise was standard Gaussian. Data were generated with sample size $n = 100$, $p_1 = 100$, and $p_2 = 1,000$ features. Note that in Feng et al. (2018), $p_2 = 10,000$. We also attempted to fit ProJIVE with $p_2 = 10,000$. However, we experienced issues with computational feasibility, and the algorithm did not converge.

3.2 Simulation results

Figures 1 and 2 summarize chordal distances between true score and loading subspaces and their estimates when simulated data conform to Gaussian assumptions in ProJIVE (level (a) of factor 4) with $r_J = 1$ and $r_J = 3$ joint component(s), respectively. For the simulations

with $p_2 = 20$ (sub-figures 1A and 2A), the joint scores were most accurate in ProJIVE across the $R_{J_k}^2$ settings, except in the small signal setting, $R_{J_1}^2 = R_{J_2}^2 = 0.1$ with $r_J = 3$ joint components. ProJIVE estimates of individual scores were more accurate than those from other methods when signal proportions were mixed, i.e., $R_{J_1}^2 \neq R_{J_2}^2$ and at least as accurate as others when signal proportions were equal across data blocks.

In the mixed-dimension setting ($p_2 = 200$; sub-figures 1B and 2B), ProJIVE achieves substantial improvement in estimating joint and individual scores and individual loadings, and moderate improvement or similar performance in joint loadings compared to other methods.

Figures 3 and 4 summarize chordal distances for simulations when joint scores were from a mixture of Gaussians and loadings from a Rademacher distribution (setting (b) of factor 4), with $r_J = 1$ and $r_J = 3$ joint component(s), respectively. For $r_J = 1$ (figure 3), ProJIVE estimates of scores and individual loadings were markedly more accurate than those from other methods when signal proportions differ and as accurate as other methods when signal proportions are equal across data sets. Chordal distances between estimated and true subspaces tended to be larger when $r_J = 3$ in these settings. However, ProJIVE estimates of joint and individual scores were generally the most accurate (figure 4). We note that joint scores and joint loadings from all methods were inaccurate when $R_{J_1}^2 = R_{J_2}^2 = 0.1$ and $p_2 = 20$. Yet, ProJIVE improves when $p_2 = 200$. In particular, when $p_2 = 200$ and $R_{J_2}^2 = 0.5$, ProJIVE leverages the information in the second dataset, and the joint scores have substantially lower chordal norms than the other methods (figure 4). Overall, the loadings are estimated with greater or similar accuracy in ProJIVE than in other methods. However, the discrepancies between ProJIVE-Oracle and ProJIVE indicate that our method is sensitive to initial values. These results suggest that ProJIVE may still be preferred even when the data are not generated from the ProJIVE model (1).

In the simulations based on the [Feng et al. \(2018\)](#) design, ProJIVE estimates of scores

had lower chordal norms than those from other methods, and ProJIVE-estimated loadings had smaller or equal chordal norms compared to other methods (Figure 5).

4 Joint Analysis of Brain Morphometry and Cognition in ADNI Data

Our data application examines shared variability in measures of cognition/behavior and brain morphometry. Data were obtained from The Alzheimer’s Disease Prediction Of Longitudinal Evolution (TADPOLE) Challenge (<https://tadpole.grand-challenge.org/>). The TADPOLE Challenge was an open competition to predict the onset of symptomatic AD in the short to medium term in an age group at risk for AD. We apply ProJIVE to data from $n = 587$ participants for whom the full battery of cognitive and behavioral assessments were available. This battery includes 22 scales and sub-scales from cognitive and behavioral assessments given to participants in the ADNI-GO and ADNI-2 phases of the study. Additional information is in Web Appendix E.1, including Table S.1 summarizing age, gender, and ApoE4 (0=negative, 1=heterozygous, and 2=homozygous) stratified by diagnosis.

4.1 Cognition

Cognitive and behavioral measures included the following assessments, each of which is represented by a single variable except where noted: 1) Clinical Dementia Rating - Sum of Boxes (CDR-SB) (higher=worse cognition); 2) Alzheimer’s Disease Assessment Scale - Cognition (ADAS), in which the 11-item and 13-item scores were used as separate variables (higher=worse cognition); 3) the Mini-Mental State Exam (MMSE) (higher=better cognition); 4) Rey’s Auditory Verbal Learning Test (RAVLT), in which Forgetting, Immediate, and Learning sub-scales were used as separate variables (higher=better cognition); 5) Mon-

trial Cognitive Assessment (MOCA) (higher=better cognition); and 6) Everyday Cognition (ECOG) (Farias et al., 2008), in which seven pairs of sub-scales were used (higher=worse cognition). Summary statistics for each of the $p_1 = 22$ cognition measures used in JIVE analyses are shown in Web Appendix Table S.2. Some cognitive measures were used to inform diagnoses (e.g., ADAS13, MOCA, and MMSE).

4.2 Brain morphometry

We used brain morphometry measures in the TADPOLE data, which were preprocessed using the cross-sectional Freesurfer pipeline (Reuter et al., 2010). The brain morphometry dataset contains measures of cortical thickness (CT), cortical surface area (SA), and cortical volume (CVol) for each of the thirty-four Desikan cortical surface ROIs (Desikan et al., 2006), as well as the volumes for the following: eight subcortical ROIs in each hemisphere, the brainstem, ventricles, cerebrospinal fluid, optic chiasm, corpus callosum, and total intracranial volume. We refer to all non-cortical regions as “sub-cortical” (SVol). In total, 245 measures of brain morphometry are included in ProJIVE and as a single dataset.

We also repeated the analysis, treating each set of measures as a separate dataset (CT, SA, CVol, and SVol), as described in Section 4.6.

4.3 Dimension reduction, preprocessing, and summary

For each feature (e.g., brain morphometry or cognition measure), we fit a linear regression with age and sex as predictors, extracted the residuals, and then standardized to have unit variance. We then inspected scree plots and selected $r_{Cog} = 5$ total components in the cognition dataset and $r_B = 12$ in the brain morphometry datasets (Web Appendix Figure S.1). The relatively small ranks are based on our previous experience that larger ranks can create issues when selecting the joint rank.

4.4 Joint subspace

A permutation test based on permuting the participants in the second dataset to generate a null distribution of the canonical correlations between principal component scores (Murden et al., 2022) resulted in one joint component, and the test of principal angles from AJIVE also resulted in one component (Feng et al., 2018).

4.4.1 Variable loadings

Joint loadings for a dataset indicate the extent to which each measure in that dataset contributes to the shared subspace. To aid interpretation, we scaled joint loadings by the reciprocal of the maximum absolute value across data sets. We focus on the top 10 largest (in absolute value) cognition loadings and the upper 90th percentile of brain loadings.

Figure 6 shows the most prominent cognition loadings include ADAS, MMSE, and MOCA, which were used for diagnosis. Lower MOCA and MMSE scores and higher ADAS, CDRSB, and ECOG scores represent worse cognitive performance. Their loadings point in opposite directions.

Measures of cortical thickness (CT) and subcortical volume (SVol) were prominent in morphometry. The loadings for subcortical volumes in the upper 90th percentile of all loadings occur within left-right pairs, including the hippocampus (Figure 6). Results were similar for left-right cortical thickness pairs, including the entorhinal cortex (Figure 7). No surface area measurements were in the upper 90th percentile. Brain loadings were consistent with associations between specific ROIs and AD found in the literature. The atrophy of gray matter structures, including the hippocampus, amygdala, and entorhinal cortex increases the risk of AD (Nestor et al., 2008; Frisoni et al., 2009; Poulin et al., 2011). The ventricles are not gray matter structures, and larger ventricles indicate greater atrophy. Consistent with this biology, they load in the opposite direction of the gray matter regions.

4.4.2 Subject scores

We examined the relationship between subject scores and genetic risk factors (ApoE4), diagnosis, and PET biomarkers (AV45 and FDG). The location of the distribution of joint scores increased in ApoE4=1 relative to ApoE4=0, and then there was a small increase in ApoE4=2 relative to ApoE4=1, although in all cases we see overlapping distributions (Figure 8). Using multinomial logistic regressions, joint subject scores were significantly related to the odds of having the ApoE4 allele ($z=5.52$, $p < 10^{-7}$ for 1 versus 0 and $z=4.78$, $p < 10^{-5}$ for 2 versus 0 allele counts, McFadden’s pseudo- $R^2 = 0.03$).

For diagnosis, we also see an increase in the location of the distribution of joint scores for CN versus MCI, and then a more substantial increase from MCI to AD with non-overlapping interquartile ranges. Joint scores were significant in the multinomial regression ($z=6.43$, $p < 10^{-9}$, and $z=11.40$, $p < 10^{-10}$ for MCI versus CN and AD versus CN, respectively, McFadden’s pseudo- $R^2=0.20$). These results indicate that the joint subject scores capture variation shared between cognition and brain morphometry, which is significantly associated with diagnoses.

Lastly, joint subject scores were significantly associated with biomarkers derived from AV-45 PET ($t=10.03$, $p < 10^{-15}$, $R^2 = 0.15$) and FDG PET ($t=-15.50$, $p < 10^{-15}$, $R^2 = 0.29$) using simple linear regression (Figure 8). Previous studies have shown that the accumulation of beta-amyloid as measured by AV-45 PET increases the risk for AD (Camus et al., 2012), while lower FDG levels are associated with dementia (Langbaum et al., 2009). PET imaging utilizes a radioactive tracer, which is more expensive and invasive than MRI. These results indicate that a significant portion of the information captured in PET biomarkers is contained in the joint subject scores of MRI and cognition data.

4.5 Individual subspaces

4.5.1 Variable loadings

Loadings for the first two components of the individual subspace of cognition were dominated by ECOG measures, with primarily self-reported measures for the first component and study partner-reported measures for the second (Web Appendix Figure S.2). RAVLT-immediate, RAVLT-learning, ADAS13, and ADAS11 loaded most strongly onto the third component, while ECOG self-reported memory dominated the fourth component. The 90th percentile of loadings for the first individual component of brain morphometry mainly consisted of surface area measures, which were not prominent in the joint subspace. Additional components are discussed in Web Appendix E.3 and displayed in Web Appendix Figure S.3.

4.5.2 Subject scores

Scores from the first three individual cognition components were associated with diagnosis, with the third component exhibited the strongest association ($z=8.79$, $p < 10^{-8}$, and $z=-5.02$, $p < 10^{-10}$, respectively, for MCI versus CN and AD versus CN, adjusted pseudo- $R^2=0.13$). The third individual cognition scores were also associated with ApoE4 ($z=3.57$, $p < 10^{-3}$ for 1 versus 0 allele counts and $z=-6.32$, $p < 10^{-9}$ for 2 versus 0 allele counts, adjusted pseudo- $R^2=0.03$), and most strongly associated with AV45 ($t = 8.82$, $p < 10^{-10}$, $R^2 = 0.12$) and FDG ($t = -6.23$, $p < 10^{-9}$, $R^2 = 0.06$). On the other hand, no individual brain morphometry scores were associated with diagnosis, ApoE4 allele counts, or AV45, while the seventh individual morphometry scores were associated with FDG ($t = -4.1$, $p < 10^{-4}$, $R^2 = 0.03$).

4.6 Alternative specification with five datasets

We conducted a similar analysis treating each collection of brain morphometry measures (i.e., CT, CVol, SA, and SVol) as a separate dataset, resulting in $K = 5$ datasets. Scree plot analyses were again employed to choose the total signal rank for each data set, which resulted in ranks of 5 for cognition, 10 for cortical thickness, 9 for cortical volume, 12 for surface area, and 10 for subcortical volume. The joint rank was chosen as $r_J = 1$ to facilitate comparison to the analysis with $K = 2$ datasets. We focus on the joint subspaces here and provide additional information about individual subspaces in the Web Appendix.

Joint subject scores from the $K = 5$ setting had a similar association to ApoE4 and diagnosis as in the $K = 2$ case, with McFadden’s pseudo- R^2 values of 0.04 and 0.21, respectively. Similarly, associations between joint scores and PET biomarkers were similar to those in the $K = 2$ case, with pseudo- R^2 values of 0.15 for AV45 and 0.26 for FDG (Web Appendix Figure S.7).

5 Discussion

We propose ProJIVE, a statistical model and novel EM algorithm for data integration that extends probabilistic PCA (Tipping and Bishop, 1999) to multiple datasets. In probabilistic PCA, there is an equivalence between the MLE and the principal subspace of classic PCA. In contrast, ProJIVE leads to novel estimators distinct from AJIVE, R.JIVE, and other data integration methods. Our simulations demonstrate that ProJIVE improves estimation of joint subject scores. ProJIVE assumes mutual orthogonality between joint and individual subject scores. Arguably, defining orthogonality on these random variables may be easier to understand for some people than assumptions on row spaces. We analyze brain morphometry and cognition in ADNI datasets. The joint subject scores were associated with ApoE4,

diagnosis, and PET biomarkers. The largest joint variable loadings show patterns that are consistent with associations found in the literature between measures of cognition, brain morphometry, and Alzheimer’s disease (Kim et al., 2015; Piers, 2018; Sultana et al., 2024). On the other hand, we find that no individual brain morphometry components were related to ApoE4 or diagnosis. This suggests the relationship between ApoE4 and brain morphometry, and the relationship between diagnosis and brain morphometry, is due to shared variation in the brain morphometry and cognition data. We found that each of the individual cognition components were related to diagnosis, which suggests information pertinent to diagnosis is partly, but not entirely, captured by brain morphometry.

ProJIVE has a number of limitations. In simulations, the computational costs were greater than AJIVE and D-CCA, but less than R.JIVE and GIPCA in the mixed dimension settings (i.e., $p_2 = 20$). AJIVE and D-CCA run times were typically less than one second when ranks were specified. Moreover, our current implementation of ProJIVE in R was not computationally feasible for the simulation setting with $p_2 = 10,000$ (see Section 3.1). While ProJIVE run times were often slower than R.JIVE and GIPCA in the high-dimensional settings, ProJIVE estimates tended to be more accurate than other methods. Additionally, we used scree plots to determine the total ranks of each dataset and a permutation test to determine the joint rank. Since we define a likelihood, one can use information criteria to determine ranks. The ProJIVE R implementation also calculates the Akaike Information Criterion (AIC) and Bayesian Information Criterion (BIC), which can be used to guide total and joint rank choices. However, this involves all combinations of r_J, r_{I_k} for $k = 1, \dots, K$, which is challenging at best.

Care must also be given to the decision of what constitutes a “dataset.” One view is outlined in Zhu et al. (2020), who suggest defining a dataset as a collection of variables that all follow a similar probability distribution. In our framework, all scores are assumed

to be Gaussian, although our simulations include settings where ProJIVE is robust to this assumption. We recommend careful consideration of the scientific impact of the datasets' definitions, for example, through evaluating multiple approaches. Treating the brain morphology as a single dataset, as presented in the main analysis (Figures 6, 7, 8), or treating each grouping as a separate dataset, as presented in the Web Appendix (Figures S.6 and S.7), had relatively minor impacts on the joint scores.

Future work could extend ProJIVE to non-Gaussian settings. In independent factor analysis, the source distributions are modeled using a mixture of Gaussians [Attias \(1999\)](#). The independent factor analysis likelihood could be extended to joint and individual components. However, the likelihood is difficult to maximize. Another direction for future research is to model observations from multiple datasets as a mixture of ProJIVE models. An EM algorithm could be developed for this setting, which would include latent variables for class membership. This would enable high dimensional clustering.

Acknowledgments

This work uses the TADPOLE data sets <https://tadpole.grand-challenge.org> constructed by the EuroPOND consortium <http://europond.eu> funded by the European Union's Horizon 2020 research and innovation programme under grant agreement No 666992. Data used in preparation of this article were obtained from the Alzheimer's Disease Neuroimaging Initiative (ADNI) database (<http://adni.loni.usc.edu>). As such, the investigators within the ADNI contributed to the design and implementation of ADNI and/or provided data but did not participate in the analyses or writing of this report. A complete listing of ADNI investigators can be found at: http://adni.loni.usc.edu/wp-content/uploads/how_to_apply/ADNI_Acknowledgement_List.pdf. The authors thank members of the Center for Biomedical Imaging Statistics (CBIS) at Emory University. This study

was supported by R21AG066970 (B.R. and D.Q.), R21AG064405 (D.Q.), R01AG072603 (D.Q.), R01MH129855 (B.R.), and an ADRC pilot grant (D.Q. and B.R.) from parent grant P30AG066511.

Declaration of Interest

No authors have conflicting interests.

Web Appendix

Supporting information referenced in Sections 2, 4, and 5 is available with this paper on the Journal of Computational and Graphical Statistics website. R code reproducing simulations is available at <https://github.com/thebrisklab/ProJIVE>.

References

- Allen, N. E., Sudlow, C., Peakman, T., Collins, R., et al. (2014). Uk biobank data: come and get it.
- Attias, H. (1999). Independent factor analysis. *Neural computation*, 11(4):803–851.
- Bishop, C. M. (1999). Ppca. *Journal of the Royal Statistical Society: Series B (Statistical Methodology)*, 61(3):611–622.
- Browne, M. W. (1979). The maximum-likelihood solution in inter-battery factor analysis. *British Journal of Mathematical and Statistical Psychology*, 32(1):75–86.
- Camus, V., Payoux, P., Barré, L., Desgranges, B., Voisin, T., Tauber, C., La Joie, R., Tafani, M., Hommet, C., Chételat, G., et al. (2012). Using pet with 18 f-av-45 (florbetapir)

- to quantify brain amyloid load in a clinical environment. *European journal of nuclear medicine and molecular imaging*, 39(4):621–631.
- Desikan, R. S., Ségonne, F., Fischl, B., Quinn, B. T., Dickerson, B. C., Blacker, D., Buckner, R. L., Dale, A. M., Maguire, R. P., Hyman, B. T., and others (2006). An automated labeling system for subdividing the human cerebral cortex on MRI scans into gyral based regions of interest. *Neuroimage*, 31(3):968–980.
- Farias, S. T., Mungas, D., Reed, B. R., Cahn-Weiner, D., Jagust, W., Baynes, K., and DeCarli, C. (2008). The measurement of everyday cognition (ecog): scale development and psychometric properties. *Neuropsychology*, 22(4):531.
- Feng, Q., Jiang, M., Hannig, J., and Marron, J. S. (2018). Angle-based joint and individual variation explained. *Journal of Multivariate Analysis*, 166:241–265.
- Frisoni, G. B., Prestia, A., Rasser, P. E., Bonetti, M., and Thompson, P. M. (2009). In vivo mapping of incremental cortical atrophy from incipient to overt alzheimer’s disease. *Journal of neurology*, 256(6):916–924.
- Gaynanova, I. and Li, G. (2019). Structural learning and integrative decomposition of multi-view data. *Biometrics*, 75(4):1121–1132.
- Hotelling, H. (1936). Relations between two sets of variates. *Biometrika*, 28(3):321–377.
- Kaiser, H. F. (1959). Computer program for varimax rotation in factor analysis. *Educational and psychological measurement*, 19(3):413–420.
- Kashyap, R., Kong, R., Bhattacharjee, S., Li, J., Zhou, J., and Thomas Yeo, B. T. (2019). Individual-specific fMRI-Subspaces improve functional connectivity prediction of behavior. *NeuroImage*, 189:804–812.

- Kim, Y. J., Cho, H., Kim, Y. J., Ki, C.-S., Chung, S. J., Ye, B. S., Kim, H. J., Kim, J.-H., Kim, S. T., Lee, K. H., et al. (2015). Apolipoprotein e4 affects topographical changes in hippocampal and cortical atrophy in alzheimer’s disease dementia: A five-year longitudinal study. *Journal of Alzheimer’s Disease*, 44(4):1075–1085.
- Klami, A., Virtanen, S., and Kaski, S. (2013). Bayesian Canonical Correlation Analysis. *Journal of Machine Learning Research*, 14:965–1003.
- Klami, A., Virtanen, S., Leppäaho, E., and Kaski, S. (2014). Group factor analysis. *IEEE transactions on neural networks and learning systems*, 26(9):2136–2147.
- Langbaum, J. B., Chen, K., Lee, W., Reschke, C., Bandy, D., Fleisher, A. S., Alexander, G. E., Foster, N. L., Weiner, M. W., Koeppe, R. A., et al. (2009). Categorical and correlational analyses of baseline fluorodeoxyglucose positron emission tomography images from the alzheimer’s disease neuroimaging initiative (adni). *Neuroimage*, 45(4):1107–1116.
- Lawley, D. N. and Maxwell, A. E. (1962). Factor analysis as a statistical method. *Journal of the Royal Statistical Society. Series D (The Statistician)*, 12(3):209–229.
- Lock, E. F., Hoadley, K. A., Marron, J. S., Nobel, A. B., Hill, C., Hoadley, K. A., Hill, C., Nobel, A. B., Marron, J. S., and Nobel, A. B. (2013). Joint and individual variation explained (JIVE) for integrated analysis of multiple data types. *Annals of Applied Statistics*, 7(1):523–542.
- Mueller, S. G., Weiner, M. W., Thal, L. J., Petersen, R. C., Jack, C. R., Jagust, W., Trojanowski, J. Q., Toga, A. W., and Beckett, L. (2005). Ways toward an early diagnosis in Alzheimer’s disease: The Alzheimer’s Disease Neuroimaging Initiative (ADNI). *Alzheimer’s and Dementia*, 46(2):55–66.

- Murden, R., Zhang, Z., Guo, Y., and Risk, B. (2022). Interpretive jive: Connections with cca and an application to brain connectivity. In Review.
- Nestor, S. M., Rupsingh, R., Borrie, M., Smith, M., Accomazzi, V., Wells, J. L., Fogarty, J., Bartha, R., and the Alzheimer’s Disease Neuroimaging Initiative (2008). Ventricular enlargement as a possible measure of Alzheimer’s disease progression validated using the Alzheimer’s disease neuroimaging initiative database. *Brain*, 131(9):2443–2454.
- O’Connell, M. J. and Lock, E. F. (2016). R.jive for exploration of multi-source molecular data. *Bioinformatics*, 32(18):2877–2879.
- Piers, R. J. (2018). Structural brain volume differences between cognitively intact apoe4 carriers and non-carriers across the lifespan. *Neural Regeneration Research*, 13(8):1309.
- Poulin, S. P., Dautoff, R., Morris, J. C., Barrett, L. F., Dickerson, B. C., Initiative, A. D. N., et al. (2011). Amygdala atrophy is prominent in early alzheimer’s disease and relates to symptom severity. *Psychiatry Research: Neuroimaging*, 194(1):7–13.
- Prothero, J., Jiang, M., Hannig, J., Tran-Dinh, Q., Ackerman, A., and Marron, J. (2024). Data integration via analysis of subspaces (divas). *TEST*, 33(3):633–674.
- Reuter, M., Rosas, H. D., and Fischl, B. (2010). Highly accurate inverse consistent registration: a robust approach. *Neuroimage*, 53(4):1181–1196.
- Risk, B. B. and Gaynanova, I. (2021). Simultaneous non-gaussian component analysis (sing) for data integration in neuroimaging. *The Annals of Applied Statistics*, 15(3):1431–1454.
- Sagonas, C., Panagakis, Y., Leidinger, A., and Zafeiriou, S. (2017). Robust joint and individual variance explained. In *2017 IEEE Conference on Computer Vision and Pattern Recognition (CVPR)*, pages 5739–5748. IEEE.

- Samorodnitsky, S., Wendt, C. H., and Lock, E. F. (2024). Bayesian simultaneous factorization and prediction using multi-omic data. *Computational Statistics & Data Analysis*, 197:107974.
- Shapiro, A. (1985). Identifiability of factor analysis: some results and open problems. *Linear Algebra and its Applications*, 70:1–7.
- Shu, H., Wang, X., and Zhu, H. (2020). D-cca: A decomposition-based canonical correlation analysis for high-dimensional datasets. *Journal of the American Statistical Association*, 115(529):292–306.
- Sui, J., Pearlson, G., Caprihan, A., Adali, T., Kiehl, K. A., Liu, J., Yamamoto, J., and Calhoun, V. D. (2011). Discriminating schizophrenia and bipolar disorder by fusing fMRI and DTI in a multimodal CCA+ joint ICA model. *NeuroImage*, 57(3).
- Sultana, O. F., Bandaru, M., Islam, M. A., and Reddy, P. H. (2024). Unraveling the complexity of human brain: Structure, function in healthy and disease states. *Ageing Research Reviews*, 100:102414.
- Tipping, M. E. and Bishop, C. M. (1999). Probabilistic principal component analysis. *Journal of the Royal Statistical Society: Series B (Statistical Methodology)*, 61(3):611–622.
- Tomczak, K., Czerwińska, P., and Wiznerowicz, M. (2015). The cancer genome atlas (tcga): an immeasurable source of knowledge. *Contemporary oncology*, 19(1A):A68.
- Tucker, L. R. (1958). An inter-battery method of factor analysis. *Psychometrika* 1958 23:2, 23(2):111–136.
- Ye, K. and Lim, L.-h. (2014). Schubert varieties and distances between subspaces of different dimensions. *SIAM Journal on Matrix Analysis and Applications*, 37(3):1176–1197.

Yu, Q., Risk, B. B., Zhang, K., and Marron, J. S. (2017). JIVE integration of imaging and behavioral data. *NeuroImage*, 152(February):38–49.

Zhou, G., Cichocki, A., Zhang, Y., and Mandic, D. P. (2016). Group Component Analysis for Multiblock Data: Common and Individual Feature Extraction. *IEEE Transactions on Neural Networks and Learning Systems*, 27(11):2426–2439.

Zhu, H., Li, G., and Lock, E. F. (2020). Generalized integrative principal component analysis for multi-type data with block-wise missing structure. *Biostatistics*, 21(2):302–318.

Figures

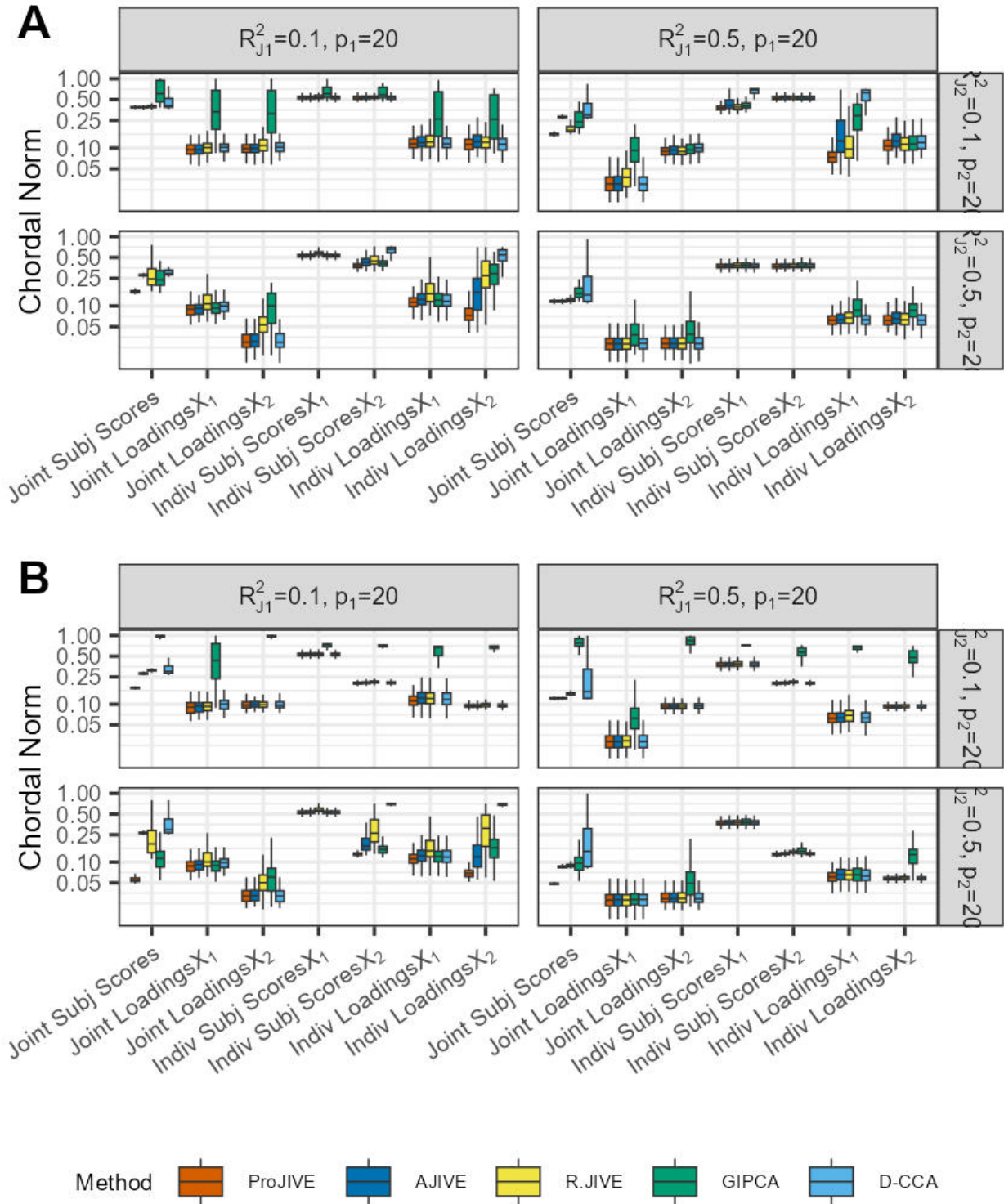


Figure 1

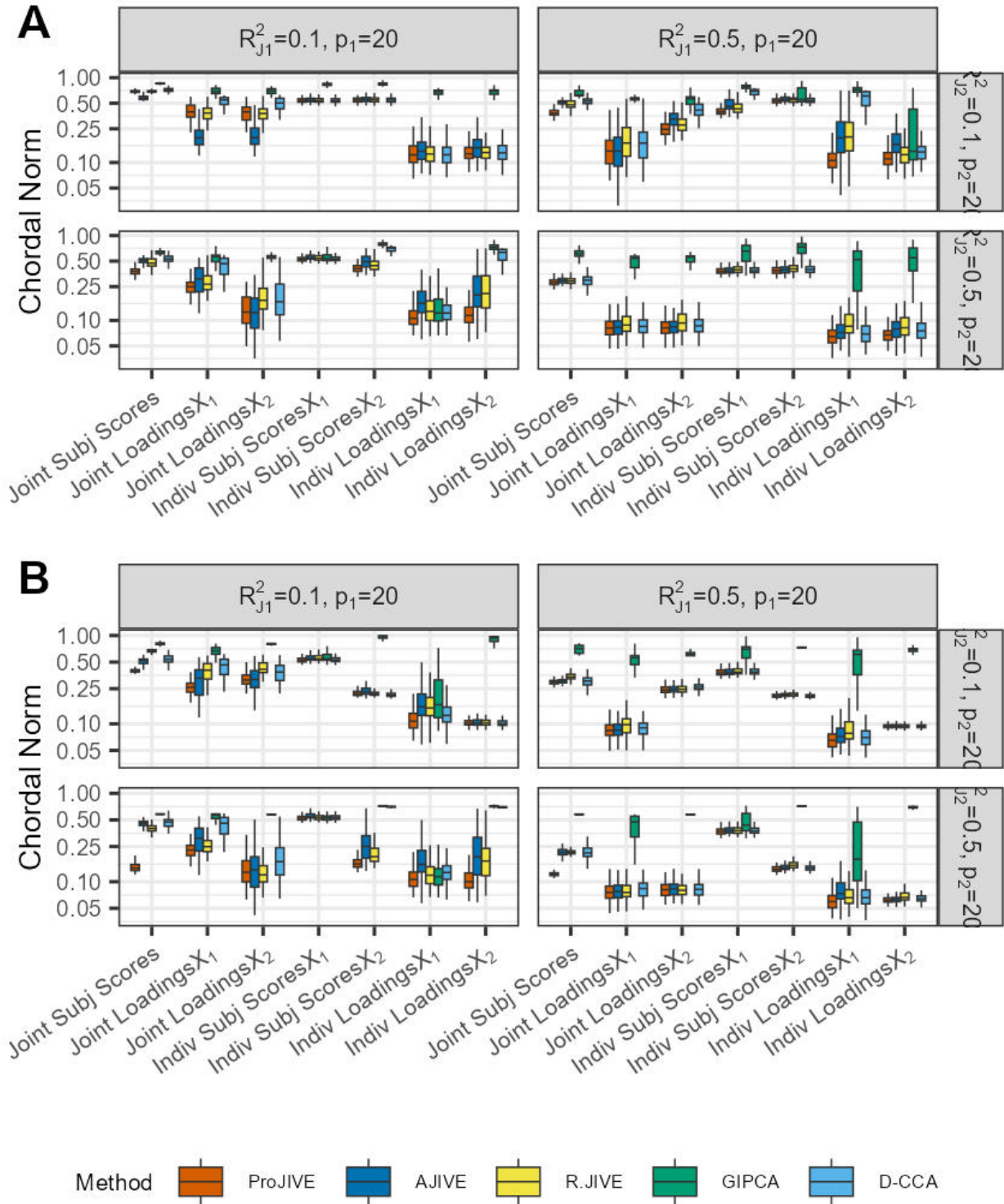


Figure 2

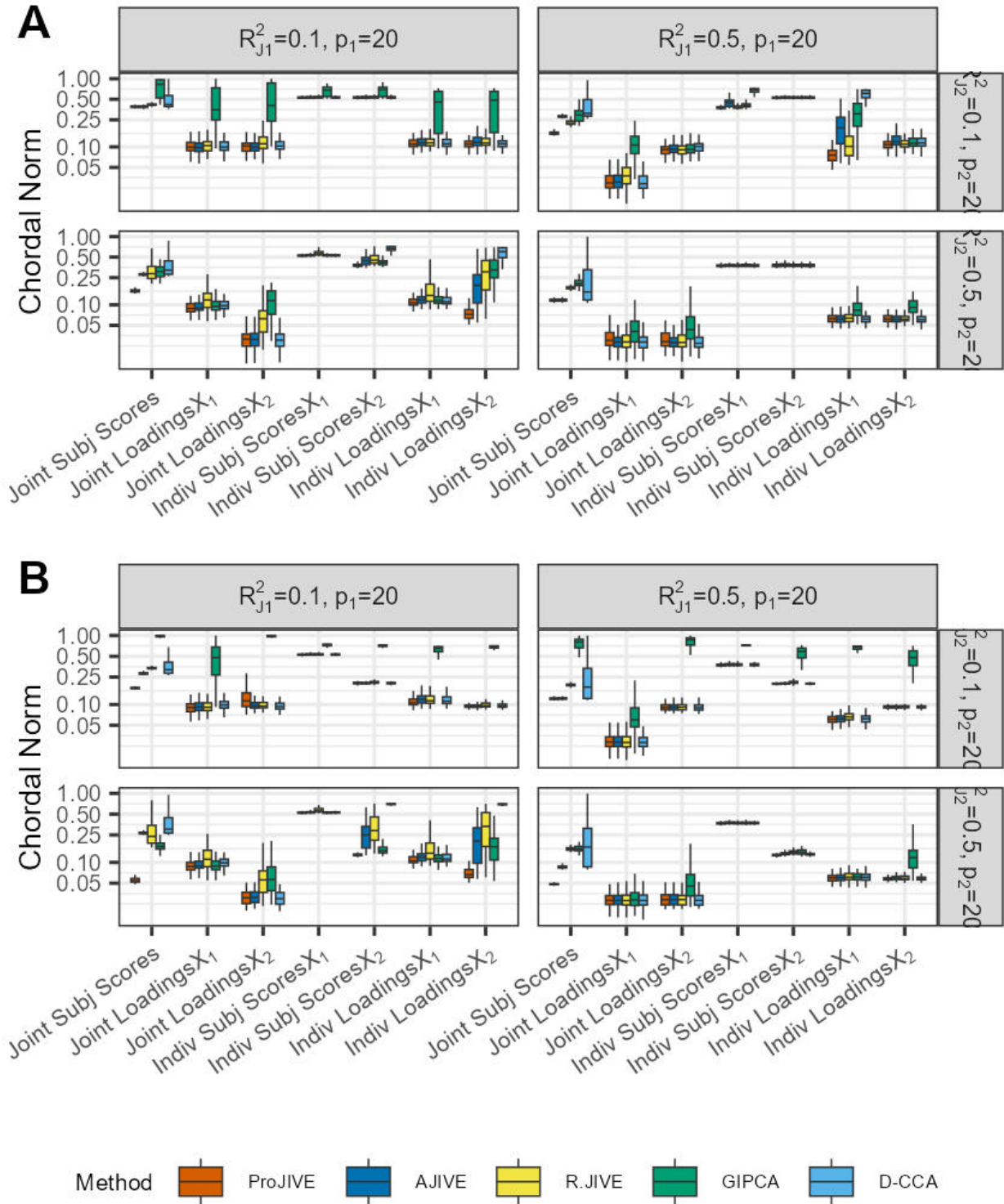


Figure 3

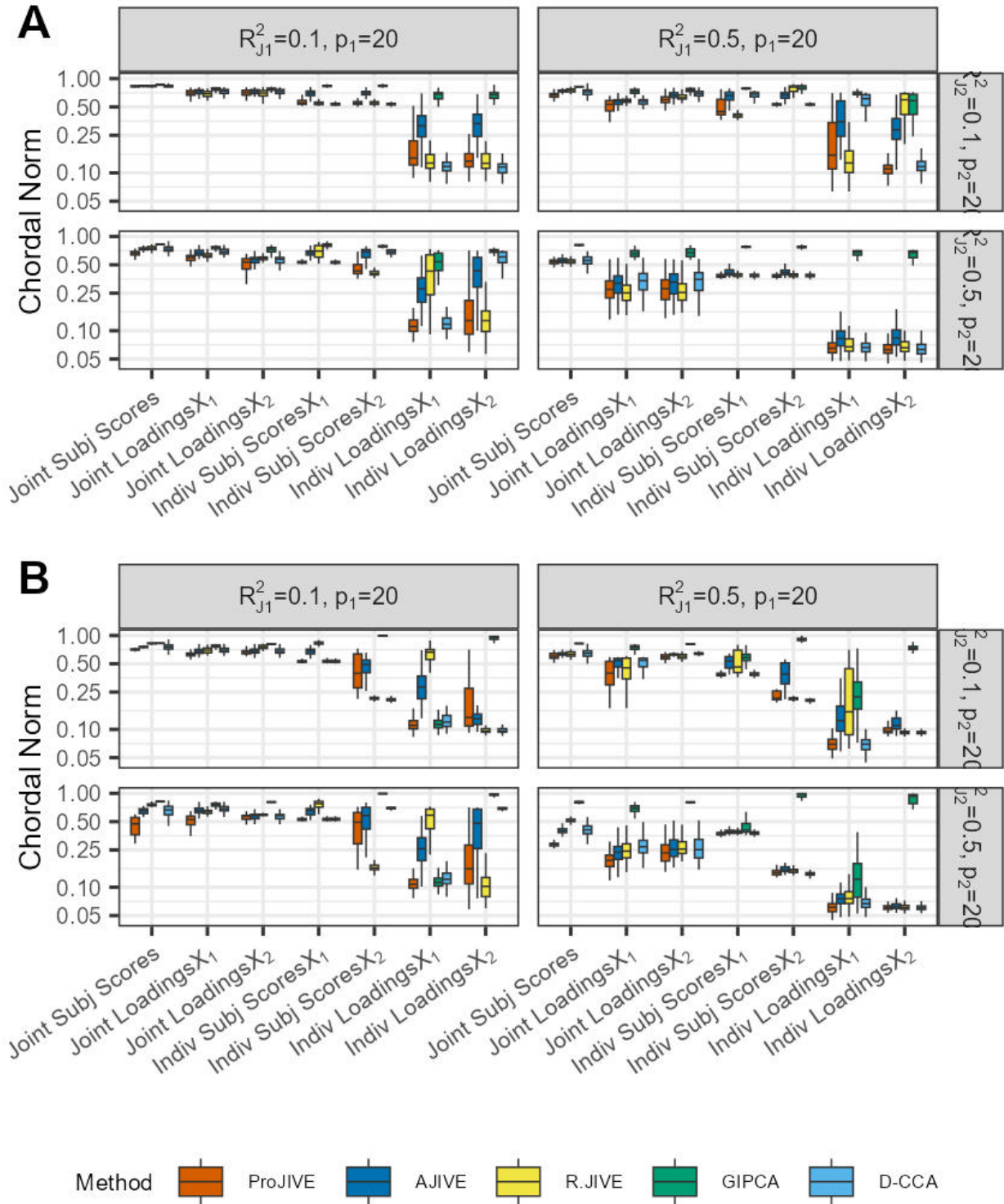


Figure 4

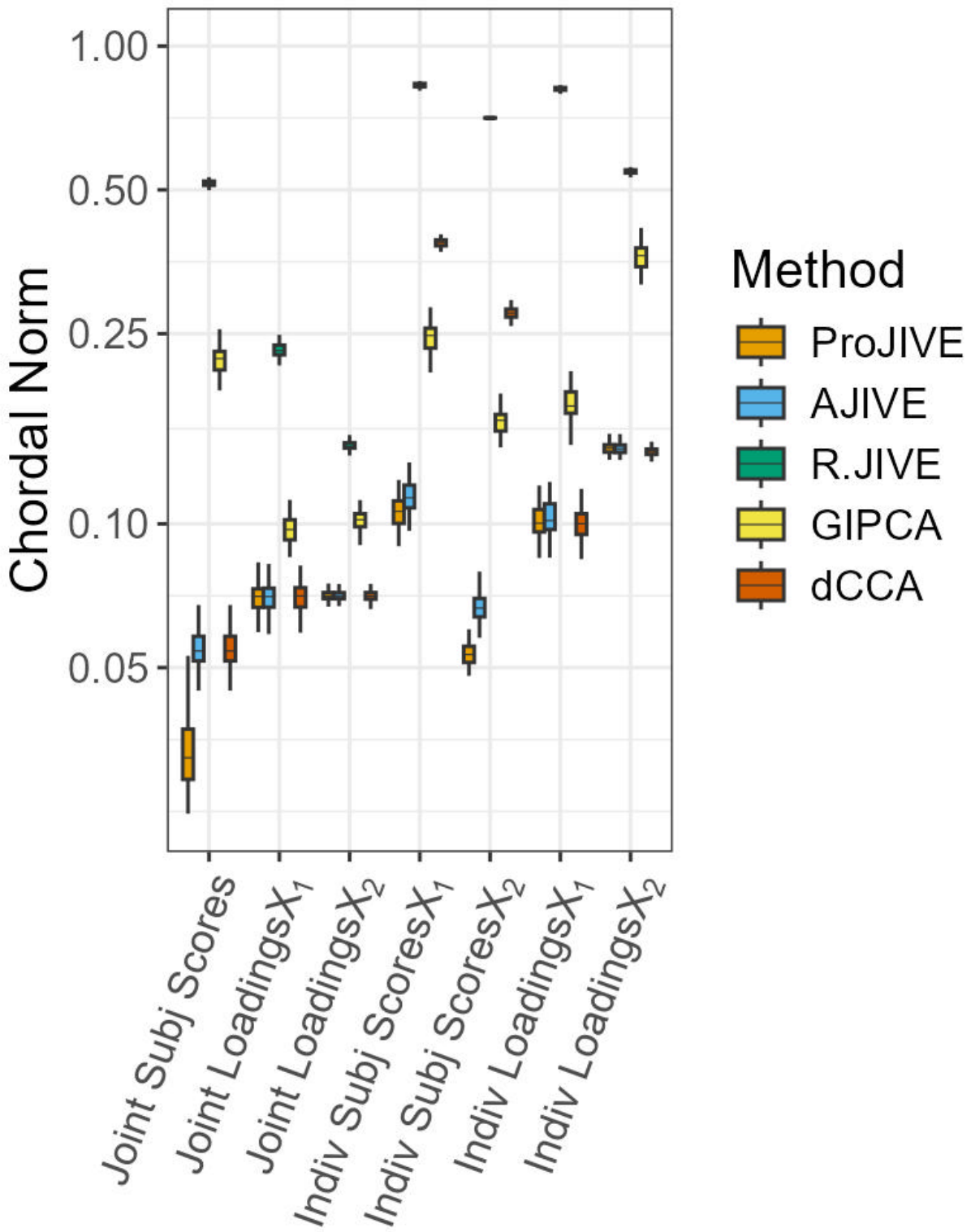


Figure 5

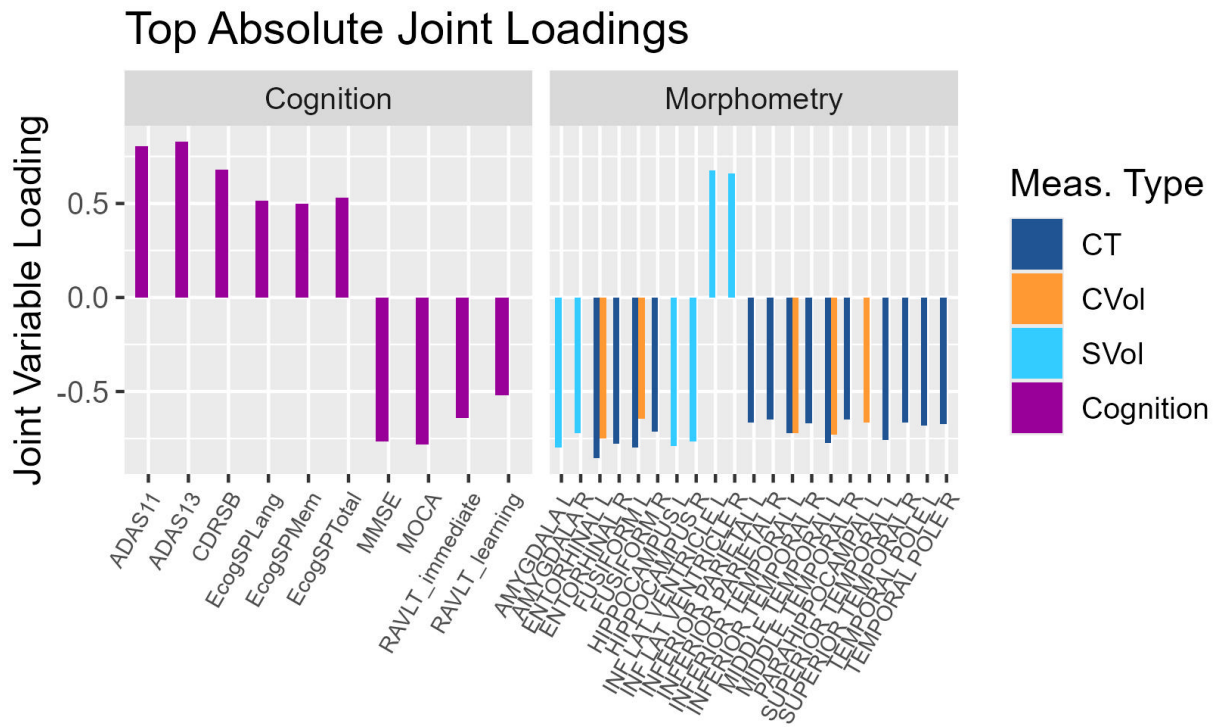


Figure 6

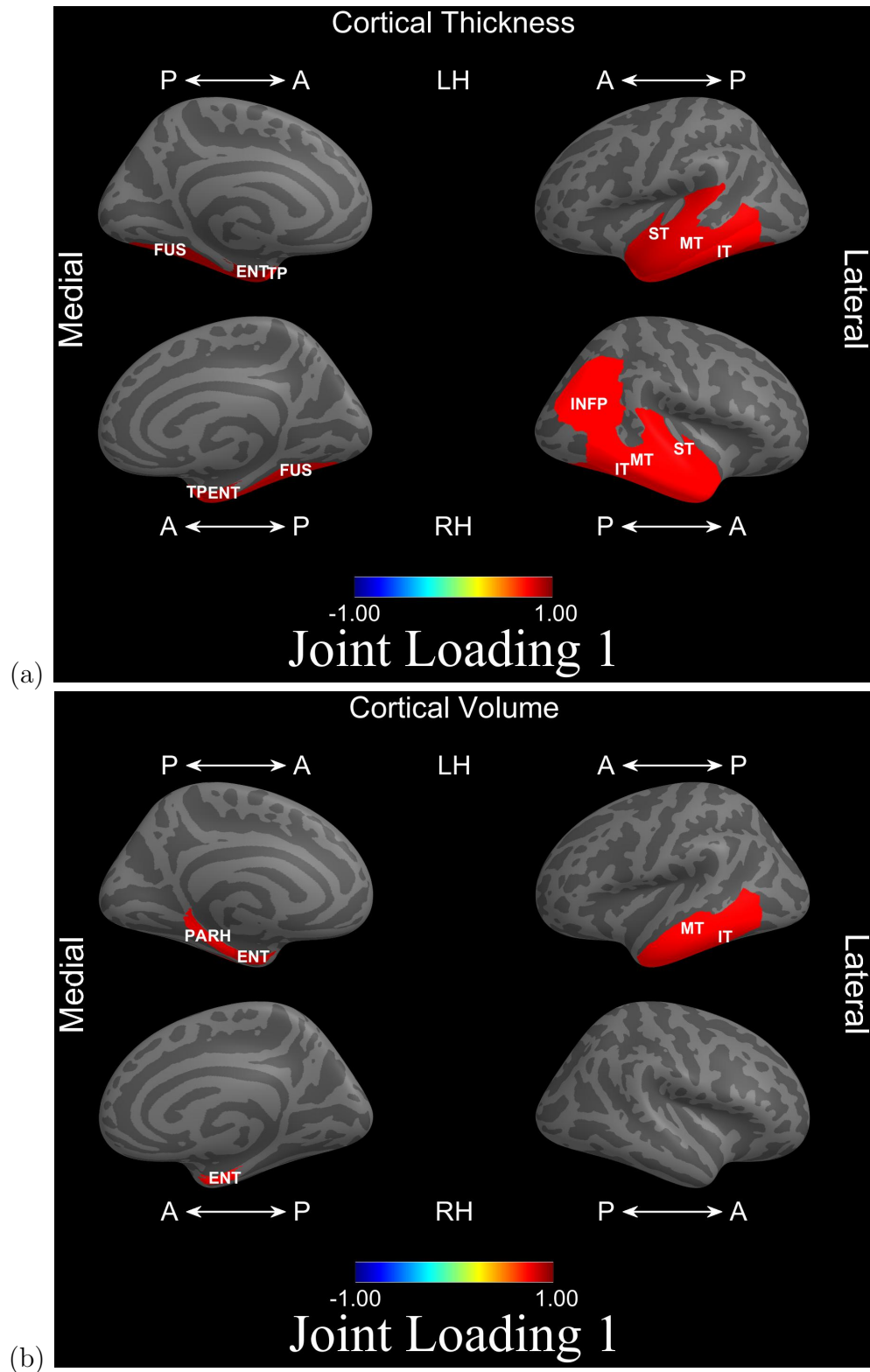


Figure 7

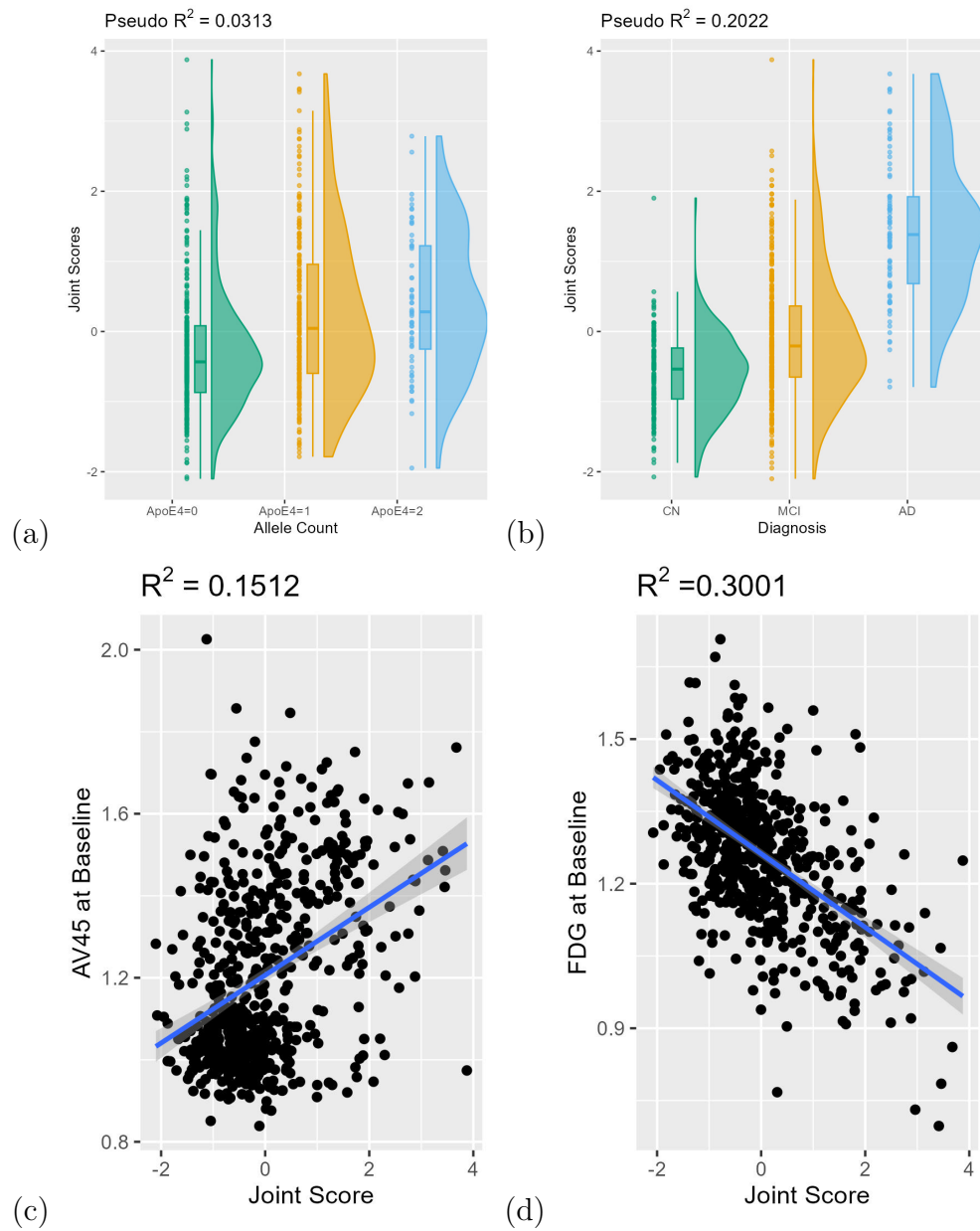


Figure 8

6 Figures Captions

- Figure 1: Interquartile and 95% intervals for chordal distances between estimated and true subspaces with data generated from the ProJIVE model with $r_J = 1$ joint component, $n = 1000$ observational units, and $p_2 = 20$ and $p_2 = 200$ in sub-figures A and B, respectively.
- Figure 2: Interquartile and 95% intervals for chordal distances between estimated and true subspaces with data generated from the ProJIVE model with $r_J = 3$ joint components, $n = 1000$ observational units, and $p_2 = 20$ and $p_2 = 200$ in sub-figures A and B, respectively.
- Figure 3: Interquartile and 95% intervals for chordal distances between estimated and true subspaces where data are generated using joint subject scores from a mixture of Gaussian distributions, individual subject scores from standard Gaussian distributions, and variable loadings (joint and individual) from Rademacher distributions with A) $p_2 = 20$, and B) $p_2 = 200$. $n = 1000$ in all settings.
- Figure 4: Interquartile and 95% intervals for chordal distances between estimated and true subspaces where data are generated using joint subject scores from a mixture of Gaussian distributions, individual subject scores from standard Gaussian distributions, and variable loadings (joint and individual) from Rademacher distributions with A) $p_2 = 20$, and B) $p_2 = 200$. $n = 1000$ in all settings.
- Figure 5: Interquartile and 95% intervals for chordal distances between estimated and true subspaces using scores and loadings based on the simulation design in [Feng et al. \(2018\)](#) with $n = 100$, $p_1 = 100$, and $p_2 = 1,000$.
- Figure 6: Variable loadings from the ten most extreme joint cognition loadings and

upper 90th percentile of the absolute value of joint brain loadings estimated via ProJIVE.

- Figure 7: Brain loadings occurring in the upper 90th percentile of the absolute value of the loadings for (a) cortical thickness and (b) cortical volume.
- Figure 8: Joint subject scores estimated via ProJIVE show separation by (a) the count of ApoE4 allele counts and (b) diagnosis via raincloud plots. (c) Scatter-plot of joint subject scores and AV45 at baseline with OLS regression line and confidence interval. (d) Scatter-plot of joint subject scores and FDG at baseline with OLS regression line and confidence interval.

Supporting Information for Probabilistic Joint and Individual Variation Explained for Data Integration

Raphael J. Murden¹, Ganzhong Tian¹, Deqiang Qiu², and Benjamin B. Risk^{*1}

¹Department of Biostatistics and Bioinformatics, Rollins School of Public Health, Emory University, 1518 Clifton Rd NE, Atlanta, GA 30322, USA

²Department of Radiology and Imaging Sciences, Emory University School of Medicine, 1364 Clifton Rd NE, Atlanta, GA 30322, USA

1 A Proof of Theorem 1

2 **Theorem 1.** *Suppose $K = 2$ and let f_{Φ} define the multivariate normal density according to*
3 *the parameters $\{\mathbf{W}_{J_1}, \mathbf{W}_{J_2}, \mathbf{W}_{I_1}, \mathbf{W}_{I_2}, \mathbf{D}_1 = \sigma_1^2 \mathbf{I}, \mathbf{D}_2 = \sigma_2^2 \mathbf{I}\}$ and the assumptions in (1)*
4 *of the main manuscript. Let f_{Φ^*} denote the multivariate normal density with parameters*
5 *$\{\mathbf{W}_{J_1}^*, \mathbf{W}_{J_2}^*, \mathbf{W}_{I_1}^*, \mathbf{W}_{I_2}^*, \mathbf{D}_1^* = \sigma_1^{*2} \mathbf{I}, \mathbf{D}_2^* = \sigma_2^{*2} \mathbf{I}\}$ and the assumptions in (1) of the main*
6 *manuscript. Then $f_{\Phi} = f_{\Phi^*}$ if and only if*

7 1. $\sigma_1^{*2} = \sigma_1^2, \sigma_2^{*2} = \sigma_2^2,$

8 2. *There exists an $r_J \times r_J$ non-singular matrix \mathbf{T}_1 such that*

9 (a) $\mathbf{W}_{J_1}^* = \mathbf{W}_{J_1} \mathbf{T}_1$ and $\mathbf{W}_{J_2}^* = \mathbf{W}_{J_2} (\mathbf{T}_1^{-1})^{\top},$

10 (b) \mathbf{T}_1 satisfies

$$\mathbf{W}_{I_1} \mathbf{W}_{I_1}^{\top} + \mathbf{W}_{J_1} (\mathbf{I} - \mathbf{T}_1 \mathbf{T}_1^{\top}) \mathbf{W}_{J_1}^{\top} \succeq 0, \quad (1)$$

$$\mathbf{W}_{I_2} \mathbf{W}_{I_2}^{\top} + \mathbf{W}_{J_2} (\mathbf{I} - (\mathbf{T}_1^{-1})^{\top} \mathbf{T}_1^{-1}) \mathbf{W}_{J_2}^{\top} \succeq 0, \quad (2)$$

*brisk@emory.edu, 1518 Clifton Rd NE, Atlanta, GA 30322

11 3. $\mathbf{W}_{I_1}^*$ is defined such that

$$\mathbf{W}_{I_1}^*(\mathbf{W}_{I_1}^*)^\top = \mathbf{W}_{I_1}\mathbf{W}_{I_1}^\top + \mathbf{W}_{J_1}(\mathbf{I} - \mathbf{T}_1\mathbf{T}_1^\top)\mathbf{W}_{J_1}^\top, \quad (3)$$

12 $\mathbf{W}_{I_2}^*$ is defined such that

$$\mathbf{W}_{I_2}^*(\mathbf{W}_{I_2}^*)^\top = \mathbf{W}_{I_2}\mathbf{W}_{I_2}^\top + \mathbf{W}_{J_2}(\mathbf{I} - (\mathbf{T}_1^{-1})^\top\mathbf{T}_1^{-1})\mathbf{W}_{J_2}^\top. \quad (4)$$

13 *Proof.* The proof builds on results from Browne (1979). It is straightforward to verify that
 14 conditions (1)–(3) result in $f_\Phi = f_{\Phi^*}$.

15 To show $f_\Phi = f_{\Phi^*}$ implies (1)–(3), let \mathbf{C}^* denote the covariance for a ProJIVE model
 16 with parameters $\{\mathbf{W}_{J_k}^*, \mathbf{W}_{I_k}^*, \sigma_k^{*2}, k = 1, 2\}$. We need to show $\mathbf{C}^* = \mathbf{C}$ implies (1)–(3).

17 First, we show $f_\Phi = f_{\Phi^*}$ implies (1). Define $\mathbf{C}_k = \text{Cov}(\mathbf{x}_{ik})$. Since \mathbf{C}_k is positive
 18 definite, we can write its eigenvalue decomposition: $\mathbf{C}_k = \mathbf{U}\Lambda\mathbf{U}^\top$, which has p_k non-zero
 19 eigenvalues. Since by assumption the noise is isotropic and $\text{rank}([\mathbf{W}_{J_k}, \mathbf{W}_{I_k}]) < p_k$, the
 20 smallest eigenvalue is equal to σ_k^2 . Let $\mathbf{C}_k^* = \text{Cov}(\mathbf{W}_{J_k}^*\mathbf{z}_i^* + \mathbf{W}_{I_k}^*\mathbf{b}_{ik}^* + \boldsymbol{\epsilon}_{ik}^*)$, where we again
 21 assume $\text{rank}(\mathbf{W}_{J_k}^* + \mathbf{W}_{I_k}^*) < p_k$. Then σ_k^{*2} is the smallest eigenvalue. Since $\mathbf{C}_k = \mathbf{C}_k^*$, the
 22 same eigenvalue decomposition applies, and we have $\sigma_k^{*2} = \sigma_k^2$.

23 Next, we will show $f_\Phi = f_{\Phi^*}$ implies (2a). Define $\mathbf{C}_{12} = \text{Cov}(\mathbf{x}_{i1}, \mathbf{x}_{i2})$. $\mathbf{C}_{12} = \mathbf{W}_{J_1}\mathbf{W}_{J_2}^\top$,
 24 and $\mathbf{C}_{12}^* = \mathbf{W}_{J_1}^*(\mathbf{W}_{J_2}^*)^\top$. By assumption, $\text{rank}(\mathbf{W}_{J_k}) = r_J$ for $k = 1, 2$, and also $\text{rank}(\mathbf{W}_{J_k}^*) =$
 25 r_J . Since $\text{rank}(\mathbf{W}_{J_2}^\top) = r_J$, $\text{rank}(\mathbf{W}_{J_1}\mathbf{W}_{J_2}^\top) = \text{rank}(\mathbf{W}_{J_1}) = r_J$. Both \mathbf{W}_{J_1} and $\mathbf{W}_{J_1}^*$ are
 26 minimal spanning sets of $\text{Col}(\mathbf{C}_{12}) = \text{Col}(\mathbf{C}_{12}^*)$. Hence there exists a change of coordi-
 27 nates matrix \mathbf{T}_1 such that $\mathbf{W}_{J_1}^* = \mathbf{W}_{J_1}\mathbf{T}_1$. The same argument applies to \mathbf{C}_{21} such that
 28 $\mathbf{W}_{J_2}^* = \mathbf{W}_{J_2}\mathbf{A}$ for some \mathbf{A} . Then we have $\mathbf{W}_{J_1}\mathbf{W}_{J_2}^\top = \mathbf{W}_{J_1}\mathbf{T}_1\mathbf{A}^\top\mathbf{W}_{J_2}^\top$. It follows that
 29 $\mathbf{W}_{J_2}^* = \mathbf{W}_{J_2}(\mathbf{T}_1^{-1})^\top$.

30 We next show $f_\Phi = f_{\Phi^*}$ implies (2b). Define $\mathbf{T}_2 = (\mathbf{T}_1^{-1})^\top$. For $k = 1, 2$, substituting
 31 $\mathbf{W}_{J_k}^* = \mathbf{W}_{J_k}\mathbf{T}_k$, we write $\mathbf{C}_k^* = \mathbf{W}_{J_k}\mathbf{T}_k\mathbf{T}_k^\top\mathbf{W}_{J_k}^\top + \text{Cov}(\mathbf{W}_{I_k}^*\mathbf{b}_{ik}^*) + \sigma_k^{*2}\mathbf{I}$. Then since $\mathbf{C}_k = \mathbf{C}_k^*$,
 32 we have $\text{Cov}(\mathbf{W}_{I_k}^*\mathbf{b}_{ik}^*) = \mathbf{W}_{I_k}\mathbf{W}_{I_k}^\top + \mathbf{W}_{J_k}(\mathbf{I} - \mathbf{T}_k\mathbf{T}_k^\top)\mathbf{W}_{J_k}^\top$. Since this must be PSD, this
 33 defines the conditions for \mathbf{T}_1 in (1) and (2).

34 Finally, $f_\Phi = f_{\Phi^*}$ implies (3) follows from the previous result that $\mathbf{C}_k^* = \mathbf{C}_k \implies$
 35 $\text{Cov}(\mathbf{W}_{Ik}^* \mathbf{b}_{ik}^*) = \mathbf{W}_{Ik} \mathbf{W}_{Ik}^\top + \mathbf{W}_{Jk} (\mathbf{I} - \mathbf{T}_k \mathbf{T}_k^\top) \mathbf{W}_{Jk}^\top.$

36 □

37 B Supplemental Information for Simulation Study

38 B.1 Proportions of Variance Explained

39 A simulation study was conducted using a 2^4 full factorial design to examine the effectiveness
 40 of ProJIVE, AJIVE, and R.JIVE for estimating the JIVE model.

41 To achieve the desired proportions of variance explained via joint and individual signals,
 42 we derive numerical solutions to:

$$R_{Ik}^2 = \frac{c_k^2 \text{tr}(\mathbf{A}_k \mathbf{A}_k^\top)}{c_k^2 \text{tr}(\mathbf{A}_k \mathbf{A}_k^\top) + 2c_k \text{tr}(\mathbf{A}_k \mathbf{E}^\top) + d_k^2 \text{tr}(\mathbf{J}_k \mathbf{J}_k^\top) + \text{tr}(\mathbf{E}_k \mathbf{E}_k^\top) + 2d_k \text{tr}(\mathbf{J}_k \mathbf{E}_k^\top)},$$

$$R_{Jk}^2 = \frac{d_k^2 \text{tr}(\mathbf{J}_k \mathbf{J}_k^\top)}{d_k^2 \text{tr}(\mathbf{J}_k \mathbf{J}_k^\top) + 2d_k \text{tr}(\mathbf{J}_k \mathbf{E}^\top) + c_k^2 \text{tr}(\mathbf{A}_k \mathbf{A}_k^\top) + \text{tr}(\mathbf{E}_k \mathbf{E}_k^\top) + 2c_k \text{tr}(\mathbf{A}_k \mathbf{E}_k^\top)}.$$

43 B.2 Chordal Subspace Norm

44 The chordal subspace norm is a distance metric for linear subspaces that has been generalized
 45 to matrices, say $\mathbf{F}_1, \mathbf{F}_2$, of possibly different ranks (Ye and Lim, 2014) and can be calculated
 46 as

$$\delta(\mathbf{F}_1, \mathbf{F}_2) = \sqrt{\sum_{m=1}^q \sin^2 \theta_m}, \quad (5)$$

47 where $q = \min_k(\text{rank}(\mathbf{F}_k))$ and θ_m are the principal angles between the column space of
 48 \mathbf{F}_1 and \mathbf{F}_2 . In practice we report $\delta^*(\mathbf{F}_1, \mathbf{F}_2) = \delta(\mathbf{F}_1, \mathbf{F}_2)/q$ so that the measure is bounded
 49 by $[0, 1]$. We use this metric in our simulation studies to describe the accuracy of JIVE
 50 estimates.

51 B.3 Tables of Gaussian Simulation Results

52 B.3.1 Joint Scores

53 Summary statistics of the chordal distance between true and estimated joint scores when
 54 data are simulated from the generative ProJIVE model. The lowest average chordal norm is
 55 displayed in bold print to indicate which method performed the best. Figures 1 and 2 in the
 56 main manuscript display box plots from the same simulations, where Figure 1 corresponds
 to rows with $r_J = 1$, and Figure 2, those with $r_J = 3$.

	r_J	P_2	$R_{J_1}^2$	$R_{J_2}^2$	ProJIVE	AJIVE	R.JIVE	GIPCA	D-CCA
					Mean (SD)				
Joint Subject Scores	1	20	0.1	0.1	0.39 (0.01)	0.39 (0.01)	0.40 (0.02)	0.68 (0.23)	0.49 (0.17)
				0.5	0.16 (0.01)	0.28 (0.01)	0.30 (0.14)	0.26 (0.08)	0.38 (0.20)
			0.5	0.1	0.16 (0.01)	0.28 (0.01)	0.20 (0.06)	0.26 (0.08)	0.39 (0.17)
				0.5	0.12 (0.00)	0.12 (0.01)	0.12 (0.01)	0.16 (0.05)	0.26 (0.23)
		200	0.1	0.1	0.17 (0.00)	0.28 (0.01)	0.31 (0.01)	0.95 (0.10)	0.35 (0.13)
				0.5	0.06 (0.01)	0.27 (0.01)	0.25 (0.17)	0.13 (0.07)	0.39 (0.19)
			0.5	0.1	0.12 (0.00)	0.12 (0.00)	0.14 (0.01)	0.71 (0.26)	0.27 (0.22)
				0.5	0.05 (0.00)	0.09 (0.00)	0.09 (0.01)	0.11 (0.08)	0.24 (0.23)
	3	20	0.1	0.1	0.69 (0.02)	0.59 (0.05)	0.69 (0.02)	0.85 (0.02)	0.71 (0.07)
				0.5	0.38 (0.04)	0.50 (0.06)	0.49 (0.08)	0.64 (0.05)	0.53 (0.07)
			0.5	0.1	0.39 (0.04)	0.50 (0.05)	0.49 (0.07)	0.66 (0.07)	0.52 (0.07)
				0.5	0.28 (0.03)	0.30 (0.03)	0.29 (0.03)	0.61 (0.07)	0.29 (0.06)
		200	0.1	0.1	0.40 (0.02)	0.50 (0.06)	0.67 (0.03)	0.80 (0.04)	0.54 (0.08)
				0.5	0.15 (0.02)	0.45 (0.05)	0.40 (0.05)	0.58 (0.01)	0.47 (0.07)
			0.5	0.1	0.30 (0.02)	0.31 (0.02)	0.34 (0.03)	0.70 (0.08)	0.30 (0.06)
				0.5	0.12 (0.01)	0.22 (0.02)	0.22 (0.01)	0.58 (0.01)	0.21 (0.04)

57

58 **B.3.2 Joint Loadings**

59 Summary statistics of the chordal distance between true and estimated joint loadings when
60 data are simulated from the generative ProJIVE model. The lowest average chordal norm is
61 displayed in bold print to indicate which method performed the best. Figures 1 and 2 in the
62 main manuscript display box plots from the same simulations, where Figure 1 corresponds
to rows with $r_J = 1$, and Figure 2, those with $r_J = 3$.

	r_J	P_2	$R_{J_1}^2$	$R_{J_2}^2$	ProJIVE	AJIVE	R.JIVE	GIPCA	D-CCA		
					Mean (SD)						
Joint Loadings X1	1	20	0.1	0.1	0.10 (0.02)	0.10 (0.02)	0.10 (0.02)	0.43 (0.30)	0.10 (0.02)		
				0.5	0.09 (0.02)	0.09 (0.02)	0.14 (0.09)	0.10 (0.03)	0.10 (0.02)		
			0.5	0.1	0.03 (0.01)	0.03 (0.01)	0.04 (0.02)	0.10 (0.05)	0.03 (0.01)		
				0.5	0.03 (0.01)	0.03 (0.01)	0.03 (0.01)	0.05 (0.02)	0.03 (0.01)		
		200	0.1	0.1	0.09 (0.02)	0.09 (0.02)	0.09 (0.02)	0.50 (0.28)	0.10 (0.02)		
				0.5	0.09 (0.02)	0.09 (0.02)	0.14 (0.10)	0.09 (0.02)	0.10 (0.02)		
			0.5	0.1	0.03 (0.01)	0.03 (0.01)	0.03 (0.01)	0.08 (0.06)	0.03 (0.01)		
				0.5	0.03 (0.01)	0.03 (0.01)	0.03 (0.01)	0.03 (0.02)	0.03 (0.01)		
		3	20	0.1	0.1	0.41 (0.09)	0.23 (0.09)	0.39 (0.08)	0.69 (0.06)	0.52 (0.09)	
					0.5	0.25 (0.05)	0.31 (0.12)	0.30 (0.11)	0.53 (0.09)	0.45 (0.11)	
				0.5	0.1	0.15 (0.07)	0.15 (0.09)	0.20 (0.10)	0.56 (0.04)	0.20 (0.12)	
					0.5	0.09 (0.03)	0.09 (0.03)	0.10 (0.04)	0.48 (0.13)	0.09 (0.03)	
	200		0.1	0.1	0.26 (0.05)	0.32 (0.12)	0.40 (0.10)	0.67 (0.07)	0.45 (0.10)		
				0.5	0.23 (0.04)	0.31 (0.11)	0.26 (0.07)	0.54 (0.06)	0.44 (0.11)		
			0.5	0.1	0.09 (0.03)	0.09 (0.03)	0.10 (0.04)	0.52 (0.13)	0.09 (0.03)		
				0.5	0.08 (0.02)	0.08 (0.02)	0.08 (0.02)	0.43 (0.13)	0.09 (0.02)		
	Joint Loadings X2		1	20	0.1	0.1	0.10 (0.02)	0.10 (0.02)	0.12 (0.04)	0.43 (0.30)	0.11 (0.02)
						0.5	0.03 (0.01)	0.03 (0.01)	0.06 (0.02)	0.10 (0.05)	0.03 (0.01)
					0.5	0.1	0.09 (0.02)	0.09 (0.02)	0.09 (0.02)	0.10 (0.02)	0.10 (0.02)
						0.5	0.03 (0.01)	0.03 (0.01)	0.03 (0.01)	0.05 (0.03)	0.03 (0.01)
		200		0.1	0.1	0.10 (0.02)	0.10 (0.02)	0.10 (0.02)	0.95 (0.10)	0.10 (0.02)	
					0.5	0.03 (0.01)	0.03 (0.01)	0.05 (0.02)	0.07 (0.04)	0.03 (0.01)	
				0.5	0.1	0.10 (0.01)	0.10 (0.01)	0.10 (0.01)	0.75 (0.28)	0.10 (0.01)	
					0.5	0.03 (0.01)	0.03 (0.01)	0.03 (0.01)	0.07 (0.05)	0.03 (0.01)	
3		20		0.1	0.1	0.40 (0.09)	0.23 (0.10)	0.38 (0.08)	0.69 (0.06)	0.50 (0.08)	
					0.5	0.14 (0.06)	0.14 (0.08)	0.21 (0.12)	0.56 (0.04)	0.20 (0.11)	
				0.5	0.1	0.25 (0.05)	0.32 (0.09)	0.30 (0.09)	0.54 (0.09)	0.43 (0.09)	
					0.5	0.09 (0.02)	0.09 (0.02)	0.10 (0.03)	0.51 (0.10)	0.09 (0.03)	
		200	0.1	0.1	0.32 (0.07)	0.32 (0.11)	0.43 (0.08)	0.79 (0.04)	0.39 (0.10)		
				0.5	0.14 (0.06)	0.15 (0.09)	0.14 (0.07)	0.58 (0.00)	0.20 (0.11)		
			0.5	0.1	0.25 (0.03)	0.25 (0.03)	0.25 (0.03)	0.64 (0.07)	0.26 (0.03)		
				0.5	0.08 (0.02)	0.09 (0.02)	0.08 (0.02)	0.58 (0.00)	0.08 (0.02)		

64 **B.3.3 Individual X_1 Scores and Loadings**

65 Summary statistics of the chordal distance between true and estimated individual scores and
66 individual loadings for data set \mathbf{X}_1 when data are simulated from the generative ProJIVE
67 model. The lowest average chordal norm is displayed in bold print to indicate which method
68 performed the best. Figures 1 and 2 in the main manuscript display box plots from the
69 same simulations, where Figure 1 corresponds to rows with $r_J = 1$, and Figure 2, those with
 $r_J = 3$.

	r_J	P_2	$R_{J_1}^2$	$R_{J_2}^2$	ProJIVE	AJIVE	R.JIVE	GIPCA	D-CCA		
					Mean (SD)						
Individual X_1 Scores	1	20	0.1	0.1	0.54 (0.04)	0.54 (0.04)	0.54 (0.04)	0.64 (0.13)	0.54 (0.04)		
				0.5	0.53 (0.04)	0.54 (0.04)	0.58 (0.05)	0.54 (0.04)	0.54 (0.04)		
			0.5	0.1	0.38 (0.04)	0.44 (0.10)	0.40 (0.06)	0.41 (0.05)	0.65 (0.10)		
				0.5	0.38 (0.04)	0.38 (0.04)	0.39 (0.04)	0.39 (0.06)	0.38 (0.04)		
		200	0.1	0.1	0.53 (0.04)	0.54 (0.04)	0.54 (0.04)	0.71 (0.07)	0.54 (0.04)		
				0.5	0.53 (0.04)	0.54 (0.04)	0.58 (0.06)	0.54 (0.04)	0.54 (0.04)		
			0.5	0.1	0.38 (0.04)	0.38 (0.04)	0.39 (0.04)	0.67 (0.13)	0.38 (0.04)		
				0.5	0.38 (0.04)	0.38 (0.04)	0.38 (0.04)	0.41 (0.11)	0.38 (0.04)		
		3	20	0.1	0.1	0.54 (0.04)	0.55 (0.04)	0.54 (0.05)	0.83 (0.05)	0.54 (0.04)	
					0.5	0.53 (0.04)	0.56 (0.05)	0.56 (0.07)	0.57 (0.10)	0.53 (0.04)	
				0.5	0.1	0.40 (0.04)	0.49 (0.10)	0.45 (0.09)	0.78 (0.06)	0.67 (0.08)	
					0.5	0.38 (0.04)	0.39 (0.04)	0.40 (0.04)	0.64 (0.16)	0.40 (0.05)	
	200		0.1	0.1	0.53 (0.04)	0.56 (0.05)	0.56 (0.05)	0.58 (0.08)	0.53 (0.04)		
				0.5	0.53 (0.04)	0.56 (0.05)	0.54 (0.06)	0.53 (0.04)	0.53 (0.04)		
			0.5	0.1	0.39 (0.04)	0.39 (0.04)	0.40 (0.04)	0.65 (0.15)	0.39 (0.04)		
				0.5	0.37 (0.04)	0.38 (0.04)	0.38 (0.04)	0.48 (0.13)	0.38 (0.04)		
	Individual Loadings X_1		1	20	0.1	0.1	0.12 (0.03)	0.13 (0.04)	0.13 (0.04)	0.37 (0.25)	0.12 (0.03)
						0.5	0.12 (0.03)	0.13 (0.04)	0.19 (0.11)	0.13 (0.05)	0.13 (0.04)
					0.5	0.1	0.08 (0.03)	0.19 (0.15)	0.14 (0.11)	0.31 (0.14)	0.56 (0.16)
						0.5	0.06 (0.02)	0.07 (0.02)	0.07 (0.02)	0.11 (0.08)	0.06 (0.02)
		200		0.1	0.1	0.12 (0.03)	0.13 (0.04)	0.13 (0.04)	0.58 (0.17)	0.12 (0.04)	
					0.5	0.12 (0.03)	0.13 (0.04)	0.19 (0.12)	0.13 (0.07)	0.13 (0.04)	
				0.5	0.1	0.06 (0.02)	0.07 (0.02)	0.07 (0.02)	0.59 (0.22)	0.07 (0.02)	
					0.5	0.06 (0.01)	0.07 (0.02)	0.07 (0.02)	0.12 (0.18)	0.07 (0.02)	
3		20		0.1	0.1	0.14 (0.08)	0.15 (0.06)	0.14 (0.07)	0.66 (0.08)	0.14 (0.07)	
					0.5	0.11 (0.03)	0.18 (0.08)	0.17 (0.15)	0.19 (0.16)	0.13 (0.05)	
				0.5	0.1	0.12 (0.05)	0.25 (0.17)	0.24 (0.15)	0.71 (0.09)	0.57 (0.14)	
					0.5	0.07 (0.02)	0.08 (0.02)	0.10 (0.04)	0.46 (0.23)	0.08 (0.06)	
		200	0.1	0.1	0.11 (0.03)	0.18 (0.08)	0.18 (0.08)	0.23 (0.16)	0.13 (0.05)		
				0.5	0.11 (0.03)	0.18 (0.08)	0.14 (0.10)	0.13 (0.05)	0.14 (0.05)		
			0.5	0.1	0.07 (0.02)	0.08 (0.02)	0.09 (0.03)	0.53 (0.21)	0.08 (0.03)		
				0.5	0.06 (0.01)	0.08 (0.03)	0.07 (0.02)	0.28 (0.21)	0.07 (0.02)		

71 **B.3.4 Individual X_2 Scores and Loadings**

72 Summary statistics of the chordal distance between true and estimated individual scores and
 73 individual loadings for data set \mathbf{X}_2 when data are simulated from the generative ProJIVE
 74 model. The lowest average chordal norm is displayed in bold print to indicate which method
 75 performed the best. Figures 1 and 2 in the main manuscript display box plots from the
 76 same simulations, where Figure 1 corresponds to rows with $r_J = 1$, and Figure 2, those with
 $r_J = 3$.

	r_J	P_2	R_{J1}^2	R_{J2}^2	ProJIVE	AJIVE	R.JIVE	GIPCA	D-CCA		
					Mean (SD)						
Individual X_2 Scores	1	20	0.1	0.1	0.53 (0.04)	0.54 (0.04)	0.54 (0.04)	0.64 (0.12)	0.54 (0.04)		
				0.5	0.38 (0.04)	0.44 (0.09)	0.47 (0.10)	0.41 (0.05)	0.63 (0.10)		
			0.5	0.1	0.53 (0.04)	0.54 (0.04)	0.53 (0.04)	0.54 (0.05)	0.53 (0.04)		
				0.5	0.38 (0.04)	0.38 (0.04)	0.38 (0.04)	0.39 (0.05)	0.38 (0.04)		
		200	0.1	0.1	0.20 (0.01)	0.21 (0.01)	0.21 (0.01)	0.69 (0.08)	0.21 (0.01)		
				0.5	0.13 (0.01)	0.20 (0.09)	0.33 (0.17)	0.16 (0.04)	0.69 (0.03)		
			0.5	0.1	0.20 (0.01)	0.20 (0.01)	0.21 (0.01)	0.53 (0.17)	0.20 (0.01)		
				0.5	0.13 (0.01)	0.13 (0.01)	0.14 (0.01)	0.16 (0.08)	0.13 (0.01)		
		3	20	0.1	0.1	0.55 (0.05)	0.56 (0.05)	0.56 (0.06)	0.84 (0.04)	0.55 (0.04)	
					0.5	0.41 (0.05)	0.50 (0.09)	0.47 (0.10)	0.79 (0.05)	0.68 (0.07)	
				0.5	0.1	0.54 (0.04)	0.56 (0.05)	0.57 (0.09)	0.62 (0.14)	0.54 (0.04)	
					0.5	0.39 (0.04)	0.40 (0.04)	0.41 (0.05)	0.70 (0.15)	0.40 (0.05)	
	200		0.1	0.1	0.22 (0.02)	0.24 (0.04)	0.22 (0.01)	0.95 (0.07)	0.21 (0.01)		
				0.5	0.17 (0.03)	0.28 (0.12)	0.21 (0.07)	0.72 (0.01)	0.70 (0.02)		
			0.5	0.1	0.21 (0.01)	0.21 (0.01)	0.22 (0.01)	0.76 (0.08)	0.21 (0.01)		
				0.5	0.14 (0.01)	0.15 (0.01)	0.16 (0.02)	0.71 (0.01)	0.14 (0.01)		
	Individual Loadings X_2		1	20	0.1	0.1	0.12 (0.03)	0.13 (0.04)	0.13 (0.04)	0.37 (0.25)	0.12 (0.03)
						0.5	0.12 (0.03)	0.13 (0.04)	0.19 (0.11)	0.13 (0.05)	0.13 (0.04)
					0.5	0.1	0.08 (0.03)	0.19 (0.15)	0.14 (0.11)	0.31 (0.14)	0.56 (0.16)
						0.5	0.06 (0.02)	0.07 (0.02)	0.07 (0.02)	0.11 (0.08)	0.06 (0.02)
		200		0.1	0.1	0.12 (0.03)	0.13 (0.04)	0.13 (0.04)	0.58 (0.17)	0.12 (0.04)	
					0.5	0.12 (0.03)	0.13 (0.04)	0.19 (0.12)	0.13 (0.07)	0.13 (0.04)	
				0.5	0.1	0.06 (0.02)	0.07 (0.02)	0.07 (0.02)	0.59 (0.22)	0.07 (0.02)	
					0.5	0.06 (0.01)	0.07 (0.02)	0.07 (0.02)	0.12 (0.18)	0.07 (0.02)	
3		20		0.1	0.1	0.14 (0.08)	0.15 (0.06)	0.14 (0.07)	0.66 (0.08)	0.14 (0.07)	
					0.5	0.11 (0.03)	0.18 (0.08)	0.17 (0.15)	0.19 (0.16)	0.13 (0.05)	
				0.5	0.1	0.12 (0.05)	0.25 (0.17)	0.24 (0.15)	0.71 (0.09)	0.57 (0.14)	
					0.5	0.07 (0.02)	0.08 (0.02)	0.10 (0.04)	0.46 (0.23)	0.08 (0.06)	
		200	0.1	0.1	0.11 (0.03)	0.18 (0.08)	0.18 (0.08)	0.23 (0.16)	0.13 (0.05)		
				0.5	0.11 (0.03)	0.18 (0.08)	0.14 (0.10)	0.13 (0.05)	0.14 (0.05)		
			0.5	0.1	0.07 (0.02)	0.08 (0.02)	0.09 (0.03)	0.53 (0.21)	0.08 (0.03)		
				0.5	0.06 (0.01)	0.08 (0.03)	0.07 (0.02)	0.28 (0.21)	0.07 (0.02)		

78 **B.4 Tables of Mixture-Rademacher Simulation Results**

79 **B.4.1 Joint Subject Scores**

80 Summary statistics of the chordal distance between true and estimated joint scores when
 81 data **are not** simulated from the generative ProJIVE model. The lowest average chordal
 82 norm is displayed in bold print to indicate which method performed the best. Figures 3
 83 and 4 in the main manuscript display box plots from the same simulations, where Figure 3
 corresponds to rows with $r_J = 1$, and Figure 4, those with $r_J = 3$.

	r_J	P_2	$R_{J_1}^2$	$R_{J_2}^2$	ProJIVE	AJIVE	R.JIVE	GIPCA	D-CCA		
Joint Subject Scores	1	20	0.1	0.1	0.39 (0.02)	0.39 (0.02)	0.42 (0.02)	0.75 (0.22)	0.51 (0.18)		
				0.5	0.16 (0.01)	0.28 (0.01)	0.33 (0.12)	0.31 (0.08)	0.43 (0.22)		
			0.5	0.1	0.16 (0.01)	0.28 (0.01)	0.23 (0.02)	0.31 (0.09)	0.42 (0.20)		
				0.5	0.12 (0.01)	0.12 (0.01)	0.18 (0.01)	0.22 (0.06)	0.28 (0.25)		
		200	0.1	0.1	0.17 (0.01)	0.28 (0.01)	0.34 (0.01)	0.97 (0.06)	0.40 (0.19)		
				0.5	0.06 (0.01)	0.27 (0.01)	0.29 (0.14)	0.18 (0.03)	0.40 (0.20)		
			0.5	0.1	0.12 (0.00)	0.12 (0.00)	0.19 (0.01)	0.72 (0.26)	0.27 (0.23)		
				0.5	0.05 (0.00)	0.09 (0.01)	0.16 (0.01)	0.16 (0.03)	0.25 (0.23)		
			3	20	0.1	0.1	0.83 (0.01)	0.83 (0.01)	0.83 (0.01)	0.86 (0.01)	0.83 (0.07)
						0.5	0.66 (0.04)	0.74 (0.03)	0.75 (0.03)	0.82 (0.02)	0.74 (0.07)
	0.5	0.1			0.66 (0.04)	0.74 (0.03)	0.75 (0.04)	0.82 (0.01)	0.72 (0.08)		
		0.5			0.54 (0.04)	0.56 (0.04)	0.55 (0.03)	0.81 (0.01)	0.54 (0.09)		
	200	0.1		0.1	0.71 (0.02)	0.76 (0.02)	0.82 (0.01)	0.83 (0.00)	0.76 (0.08)		
				0.5	0.46 (0.10)	0.65 (0.04)	0.76 (0.02)	0.82 (0.01)	0.66 (0.10)		
		0.5		0.1	0.61 (0.04)	0.64 (0.03)	0.64 (0.04)	0.82 (0.00)	0.63 (0.11)		
				0.5	0.29 (0.01)	0.40 (0.03)	0.52 (0.03)	0.80 (0.02)	0.40 (0.08)		

85 **B.4.2 Joint Loadings**

86 Summary statistics of the chordal distance between true and estimated joint loadings when
 87 **data are** simulated from the generative ProJIVE model. The lowest average chordal norm is
 88 displayed in bold print to indicate which method performed the best. Figures 3 and 4 in the
 89 main manuscript display box plots from the same simulations, where Figure 3 corresponds
 to rows with $r_J = 1$, and Figure 4, those with $r_J = 3$.

	r_J	P_2	$R_{J_1}^2$	$R_{J_2}^2$	ProJIVE	AJIVE	R.JIVE	GIPCA	D-CCA		
					Mean (SD)						
Joint Loadings X_1	1	20	0.1	0.1	0.10 (0.02)	0.10 (0.02)	0.11 (0.03)	0.48 (0.30)	0.10 (0.02)		
				0.5	0.09 (0.02)	0.09 (0.02)	0.13 (0.07)	0.11 (0.10)	0.10 (0.02)		
			0.5	0.1	0.03 (0.01)	0.03 (0.01)	0.04 (0.01)	0.12 (0.08)	0.03 (0.01)		
				0.5	0.04 (0.05)	0.03 (0.01)	0.03 (0.01)	0.05 (0.04)	0.03 (0.01)		
		200	0.1	0.1	0.09 (0.02)	0.09 (0.02)	0.09 (0.02)	0.50 (0.26)	0.10 (0.02)		
				0.5	0.09 (0.02)	0.09 (0.02)	0.13 (0.07)	0.09 (0.02)	0.10 (0.02)		
			0.5	0.1	0.03 (0.01)	0.03 (0.01)	0.03 (0.01)	0.10 (0.14)	0.03 (0.01)		
				0.5	0.03 (0.01)						
		3	20	0.1	0.1	0.70 (0.05)	0.73 (0.05)	0.69 (0.05)	0.77 (0.03)	0.73 (0.05)	
					0.5	0.59 (0.06)	0.67 (0.05)	0.63 (0.05)	0.75 (0.04)	0.69 (0.05)	
				0.5	0.1	0.51 (0.10)	0.55 (0.08)	0.57 (0.07)	0.73 (0.05)	0.55 (0.08)	
					0.5	0.29 (0.09)	0.33 (0.10)	0.26 (0.07)	0.66 (0.06)	0.35 (0.10)	
	200		0.1	0.1	0.63 (0.04)	0.68 (0.05)	0.70 (0.05)	0.77 (0.03)	0.70 (0.05)		
				0.5	0.52 (0.08)	0.65 (0.06)	0.64 (0.04)	0.76 (0.04)	0.69 (0.05)		
			0.5	0.1	0.40 (0.13)	0.51 (0.09)	0.45 (0.12)	0.75 (0.05)	0.51 (0.09)		
				0.5	0.20 (0.05)	0.25 (0.07)	0.27 (0.10)	0.68 (0.07)	0.29 (0.08)		
	Joint Loadings X_2		1	20	0.1	0.1	0.10 (0.02)	0.10 (0.02)	0.12 (0.04)	0.52 (0.31)	0.10 (0.02)
						0.5	0.03 (0.01)	0.03 (0.01)	0.07 (0.03)	0.13 (0.08)	0.03 (0.01)
					0.5	0.1	0.09 (0.02)	0.09 (0.02)	0.09 (0.02)	0.11 (0.07)	0.10 (0.02)
						0.5	0.05 (0.07)	0.03 (0.01)	0.03 (0.01)	0.05 (0.03)	0.03 (0.01)
		200		0.1	0.1	0.12 (0.04)	0.10 (0.02)	0.10 (0.02)	0.97 (0.06)	0.10 (0.01)	
					0.5	0.03 (0.01)	0.03 (0.01)	0.06 (0.03)	0.07 (0.03)	0.03 (0.01)	
				0.5	0.1	0.09 (0.01)	0.09 (0.01)	0.09 (0.01)	0.74 (0.30)	0.09 (0.01)	
					0.5	0.03 (0.01)	0.03 (0.01)	0.03 (0.01)	0.06 (0.04)	0.03 (0.01)	
3		20		0.1	0.1	0.71 (0.05)	0.72 (0.05)	0.70 (0.06)	0.77 (0.03)	0.72 (0.05)	
					0.5	0.51 (0.10)	0.55 (0.08)	0.58 (0.06)	0.73 (0.05)	0.55 (0.08)	
				0.5	0.1	0.59 (0.07)	0.67 (0.07)	0.63 (0.06)	0.75 (0.04)	0.69 (0.06)	
					0.5	0.28 (0.09)	0.33 (0.10)	0.27 (0.08)	0.68 (0.07)	0.35 (0.10)	
		200	0.1	0.1	0.67 (0.04)	0.69 (0.05)	0.76 (0.04)	0.81 (0.00)	0.69 (0.05)		
				0.5	0.54 (0.07)	0.55 (0.09)	0.59 (0.03)	0.81 (0.01)	0.55 (0.10)		
			0.5	0.1	0.59 (0.04)	0.63 (0.02)	0.60 (0.03)	0.81 (0.01)	0.64 (0.02)		
				0.5	0.25 (0.07)	0.27 (0.08)	0.28 (0.09)	0.80 (0.01)	0.27 (0.08)		

91 **B.4.3 Individual X_1 Scores and Loadings**

92 Summary statistics of the chordal distance between true and estimated individual scores and
 93 individual loadings for data set \mathbf{X}_1 when **data are** simulated from the generative ProJIVE
 94 model. The lowest average chordal norm is displayed in bold print to indicate which method
 95 performed the best. Figures 3 and 4 in the main manuscript display box plots from the
 96 same simulations, where Figure 3 corresponds to rows with $r_J = 1$, and Figure 4, those with
 97 $r_J = 3$.

	r_J	P_2	$R_{J_1}^2$	$R_{J_2}^2$	ProJIVE	AJIVE	R.JIVE	GIPCA	D-CCA		
					Mean (SD)						
Individual X_1 Scores	1	20	0.1	0.1	0.53 (0.02)	0.53 (0.02)	0.54 (0.02)	0.66 (0.11)	0.53 (0.02)		
				0.5	0.53 (0.02)	0.53 (0.02)	0.58 (0.05)	0.54 (0.03)	0.53 (0.02)		
			0.5	0.1	0.38 (0.02)	0.45 (0.06)	0.39 (0.02)	0.42 (0.06)	0.38 (0.02)		
				0.5	0.38 (0.03)	0.38 (0.02)	0.38 (0.02)	0.39 (0.06)	0.38 (0.02)		
		200	0.1	0.1	0.53 (0.02)	0.53 (0.02)	0.53 (0.02)	0.72 (0.05)	0.53 (0.02)		
				0.5	0.53 (0.02)	0.53 (0.02)	0.58 (0.06)	0.53 (0.03)	0.53 (0.02)		
			0.5	0.1	0.37 (0.02)	0.38 (0.02)	0.38 (0.02)	0.66 (0.13)	0.38 (0.02)		
				0.5	0.37 (0.01)	0.38 (0.02)	0.37 (0.02)	0.39 (0.07)	0.37 (0.02)		
		3	20	0.1	0.1	0.57 (0.06)	0.70 (0.06)	0.57 (0.08)	0.83 (0.02)	0.54 (0.02)	
					0.5	0.54 (0.04)	0.67 (0.05)	0.70 (0.10)	0.80 (0.06)	0.53 (0.02)	
				0.5	0.1	0.51 (0.13)	0.65 (0.09)	0.41 (0.03)	0.79 (0.04)	0.67 (0.05)	
					0.5	0.39 (0.04)	0.42 (0.04)	0.39 (0.02)	0.77 (0.02)	0.39 (0.02)	
	200		0.1	0.1	0.53 (0.02)	0.68 (0.05)	0.82 (0.06)	0.53 (0.02)	0.53 (0.02)		
				0.5	0.53 (0.02)	0.64 (0.06)	0.76 (0.08)	0.53 (0.02)	0.53 (0.02)		
			0.5	0.1	0.39 (0.02)	0.52 (0.08)	0.53 (0.15)	0.59 (0.09)	0.39 (0.02)		
				0.5	0.37 (0.02)	0.39 (0.03)	0.40 (0.07)	0.45 (0.09)	0.38 (0.02)		
	Individual Loadings X_1		1	20	0.1	0.1	0.11 (0.02)	0.12 (0.02)	0.12 (0.02)	0.42 (0.24)	0.11 (0.02)
						0.5	0.11 (0.02)	0.12 (0.02)	0.18 (0.11)	0.13 (0.08)	0.12 (0.02)
					0.5	0.1	0.08 (0.02)	0.20 (0.10)	0.12 (0.06)	0.32 (0.15)	0.58 (0.13)
						0.5	0.07 (0.01)	0.06 (0.01)	0.07 (0.01)	0.12 (0.12)	0.06 (0.01)
		200		0.1	0.1	0.11 (0.02)	0.12 (0.02)	0.12 (0.02)	0.60 (0.14)	0.12 (0.02)	
					0.5	0.11 (0.02)	0.12 (0.02)	0.18 (0.12)	0.12 (0.06)	0.12 (0.02)	
				0.5	0.1	0.06 (0.01)	0.06 (0.01)	0.07 (0.01)	0.57 (0.23)	0.06 (0.01)	
					0.5	0.06 (0.01)	0.06 (0.01)	0.06 (0.01)	0.09 (0.13)	0.06 (0.01)	
3		20		0.1	0.1	0.19 (0.12)	0.33 (0.12)	0.19 (0.16)	0.65 (0.08)	0.12 (0.02)	
					0.5	0.13 (0.09)	0.30 (0.12)	0.43 (0.21)	0.53 (0.16)	0.12 (0.02)	
				0.5	0.1	0.23 (0.17)	0.40 (0.19)	0.14 (0.05)	0.70 (0.07)	0.58 (0.11)	
					0.5	0.07 (0.03)	0.09 (0.03)	0.07 (0.02)	0.65 (0.07)	0.07 (0.02)	
		200	0.1	0.1	0.11 (0.02)	0.31 (0.13)	0.62 (0.14)	0.12 (0.02)	0.12 (0.02)		
				0.5	0.11 (0.02)	0.28 (0.11)	0.54 (0.17)	0.12 (0.02)	0.13 (0.02)		
			0.5	0.1	0.07 (0.01)	0.14 (0.06)	0.26 (0.21)	0.27 (0.16)	0.07 (0.02)		
				0.5	0.06 (0.01)	0.08 (0.02)	0.10 (0.10)	0.15 (0.11)	0.07 (0.01)		

98 **B.4.4 Individual X_2 Scores and Loadings**

99 Summary statistics of the chordal distance between true and estimated individual scores and
 100 individual loadings for data set \mathbf{X}_2 when **data are** simulated from the generative ProJIVE
 101 model. The lowest average chordal norm is displayed in bold print to indicate which method
 102 performed the best. Figures 3 and 4 in the main manuscript display box plots from the same
 simulations, as in section D.4.3 above.

	r_J	P_2	$R_{J_1}^2$	$R_{J_2}^2$	ProJIVE	AJIVE	R.JIVE	GIPCA	D-CCA		
					Mean (SD)						
Individual X_2 Scores	1	20	0.1	0.1	0.53 (0.02)	0.54 (0.02)	0.54 (0.02)	0.67 (0.11)	0.54 (0.02)		
				0.5	0.38 (0.02)	0.45 (0.07)	0.48 (0.09)	0.42 (0.06)	0.66 (0.06)		
			0.5	0.1	0.53 (0.02)	0.53 (0.02)	0.53 (0.02)	0.54 (0.04)	0.53 (0.02)		
				0.5	0.38 (0.03)	0.38 (0.03)	0.38 (0.02)	0.39 (0.05)	0.38 (0.02)		
		200	0.1	0.1	0.20 (0.01)	0.20 (0.01)	0.21 (0.01)	0.70 (0.05)	0.20 (0.01)		
				0.5	0.13 (0.01)	0.27 (0.12)	0.33 (0.15)	0.16 (0.03)	0.69 (0.02)		
			0.5	0.1	0.20 (0.01)	0.20 (0.01)	0.21 (0.01)	0.53 (0.18)	0.20 (0.01)		
				0.5	0.13 (0.00)	0.13 (0.01)	0.14 (0.01)	0.15 (0.03)	0.13 (0.01)		
		3	20	0.1	0.1	0.56 (0.06)	0.70 (0.06)	0.59 (0.10)	0.84 (0.03)	0.54 (0.02)	
					0.5	0.47 (0.11)	0.66 (0.09)	0.41 (0.03)	0.79 (0.03)	0.68 (0.05)	
				0.5	0.1	0.53 (0.02)	0.67 (0.06)	0.77 (0.09)	0.80 (0.07)	0.53 (0.02)	
					0.5	0.38 (0.02)	0.42 (0.04)	0.39 (0.04)	0.77 (0.02)	0.39 (0.02)	
	200		0.1	0.1	0.45 (0.18)	0.47 (0.10)	0.21 (0.01)	0.99 (0.01)	0.21 (0.01)		
				0.5	0.45 (0.18)	0.55 (0.17)	0.16 (0.02)	0.99 (0.01)	0.69 (0.02)		
			0.5	0.1	0.30 (0.17)	0.39 (0.11)	0.22 (0.07)	0.90 (0.07)	0.20 (0.01)		
				0.5	0.15 (0.01)	0.16 (0.02)	0.16 (0.05)	0.95 (0.06)	0.14 (0.01)		
	Individual Loadings X_2		1	20	0.1	0.1	0.11 (0.02)	0.12 (0.03)	0.12 (0.03)	0.42 (0.24)	0.11 (0.02)
						0.5	0.08 (0.02)	0.21 (0.11)	0.32 (0.18)	0.34 (0.14)	0.58 (0.12)
					0.5	0.1	0.11 (0.02)	0.13 (0.03)	0.11 (0.02)	0.13 (0.08)	0.12 (0.03)
						0.5	0.06 (0.01)	0.06 (0.01)	0.06 (0.01)	0.12 (0.11)	0.06 (0.01)
		200		0.1	0.1	0.09 (0.01)	0.10 (0.01)	0.10 (0.01)	0.66 (0.07)	0.10 (0.01)	
					0.5	0.07 (0.02)	0.22 (0.14)	0.35 (0.19)	0.17 (0.08)	0.69 (0.02)	
				0.5	0.1	0.09 (0.00)	0.09 (0.00)	0.09 (0.00)	0.45 (0.20)	0.09 (0.00)	
					0.5	0.06 (0.00)	0.06 (0.01)	0.06 (0.01)	0.13 (0.07)	0.06 (0.01)	
3		20		0.1	0.1	0.17 (0.11)	0.34 (0.11)	0.21 (0.19)	0.66 (0.08)	0.12 (0.02)	
					0.5	0.18 (0.14)	0.43 (0.18)	0.14 (0.06)	0.70 (0.06)	0.59 (0.10)	
				0.5	0.1	0.11 (0.02)	0.31 (0.12)	0.52 (0.19)	0.53 (0.17)	0.12 (0.02)	
					0.5	0.07 (0.01)	0.09 (0.03)	0.07 (0.06)	0.64 (0.08)	0.07 (0.01)	
		200	0.1	0.1	0.22 (0.17)	0.13 (0.02)	0.10 (0.01)	0.94 (0.05)	0.10 (0.01)		
				0.5	0.22 (0.15)	0.46 (0.21)	0.11 (0.04)	0.96 (0.03)	0.69 (0.02)		
			0.5	0.1	0.15 (0.13)	0.12 (0.02)	0.10 (0.07)	0.75 (0.07)	0.09 (0.00)		
				0.5	0.06 (0.00)	0.06 (0.01)	0.07 (0.04)	0.88 (0.11)	0.06 (0.00)		

Table S.1: Summary statistics for selected covariates of participants in ADNI-GO and ADNI2.

	AD (N=88)	MCI (N=340)	CN (N=159)	Total (N=587)	p value
	Mean (S.D.) or N (%)				
Age					0.006
	74.0 (7.92)	71.5 (7.57)	72.8 (5.85)	72.2 (7.25)	
Gender					0.006
Female	28 (31.8%)	150 (44.1%)	84 (52.8%)	262 (44.6%)	
ApoE4					<0.001
0	21 (23.9%)	178 (52.4%)	111 (69.8%)	310 (52.8%)	
1	45 (51.1%)	126 (37.1%)	46 (28.9%)	217 (37.0%)	
2	22 (25.0%)	36 (10.6%)	2 (1.3%)	60 (10.2%)	

C Supplemental information for ADNI analysis

C.1 Details of the participants

There are approximately $n = 1600$ participants in the TADPOLE datasets. We examined data from $n = 587$ participants for whom the full battery of cognitive and behavioral assessments were available. We limit our analysis to observations taken at the participants' 6-month follow-up visit to minimize missingness and maximize sample size. Both ADNI-2 and ADNI-GO limit newly recruited participants to those between 55-90 years of age and require that each has an English- or Spanish-speaking study partner to provide independent evaluation of patient functioning. ADNI-GO inclusion criteria required that participants who rolled over from ADNI-1 were either diagnosed as cognitively normal (CN) or having mild cognitive impairment (MCI) at baseline. Newly recruited participants in ADNI-GO were all diagnosed with early mild cognitive impairment (EMCI). ADNI-2 participants were either rolled-over from ADNI-1/ADNI-GO or newly recruited participants diagnosed as CN, EMCI, LMCI (late mild cognitive impairment), or AD. We combine EMCI and LMCI participants with MCI and only use diagnoses from the 6-month follow-up visit.

The cognitive measures include the following: 1) Clinical Dementia Rating - Sum of Boxes (CDR-SB) (Morris, 1997); 2) Alzheimer's Disease Assessment Scale - Cognition (ADAS) (Rosen et al., 1984), in which the 11-item and 13-item scores were used as separate variables; 3) the Mini-Mental State Exam (MMSE) (Folstein et al., 1975); 4) Rey's Auditory Verbal

123 Learning Test (RAVLT) (Rey, 1941, 1958), in which Forgetting, Immediate, and Learn-
124 ing sub-scales were used as separate variables; 5) Montreal Cognitive Assessment (MOCA)
125 (Nasreddine et al., 2005); and 6) Everyday Cognition (ECOG) (Farias et al., 2008), in which
126 seven pairs of sub-scales were used and each pair includes a response from the participant and
127 his or her study partner. Table S.2 provides summary statistics for the cognitive measures
128 that were included in our ProJIVE analyses of TADPOLE/ADNI data.

Table S.2: Summary statistics for Cognition Measures.

	AD (N=88)	MCI (N=340)	CN (N=159)	Total (N=587)	
Cognition Score	Mean (SD)				p value
CDRSB	4.8 (1.84)	1.4 (0.97)	0.1 (0.33)	1.6 (1.79)	<0.001
ADAS11	20.4 (6.52)	9.1 (4.69)	5.5 (2.76)	9.8 (6.60)	
ADAS13	30.8 (8.06)	14.3 (7.03)	8.5 (4.35)	15.2 (9.63)	<0.001
MMSE					<0.001
MMSE	23.1 (3.05)	27.8 (2.00)	29.0 (1.14)	27.4 (2.74)	<0.001
RAVLT (immediate)	20.5 (6.18)	34.7 (10.84)	42.9 (9.35)	34.8 (12.08)	<0.001
RAVLT (learning)	1.3 (1.75)	4.4 (2.51)	5.5 (2.19)	4.3 (2.67)	<0.001
RAVLT (forgetting)	4.0 (1.61)	4.7 (2.45)	4.2 (2.80)	4.46 (2.46)	0.019
MOCA	17.8 (4.36)	23.5 (3.26)	25.9 (2.45)	23.3 (4.12)	<0.001
EcogPTMem	2.4 (0.75)	2.2 (0.74)	1.6 (0.46)	2.0 (0.74)	<0.001
EcogPTLang	1.9 (0.79)	1.8 (0.64)	1.4 (0.39)	1.7 (0.65)	<0.001
EcogPTVisspat	1.7 (0.71)	1.4 (0.54)	1.1 (0.22)	1.4 (0.53)	<0.001
EcogPTPlan	1.6 (0.72)	1.5 (0.53)	1.1 (0.26)	1.4 (0.54)	<0.001
EcogPTOrgan	1.8 (0.75)	1.6 (0.61)	1.3 (0.34)	1.5 (0.60)	<0.001
EcogPTDivatt	1.98 (0.81)	1.90 (0.76)	1.45 (0.58)	1.79 (0.75)	<0.001
EcogPTTotal	1.91 (0.66)	1.74 (0.53)	1.33 (0.30)	1.65 (0.54)	<0.001
EcogSPMem	3.32 (0.63)	2.09 (0.78)	1.29 (0.36)	2.06 (0.92)	<0.001
EcogSPLang	2.63 (0.75)	1.65 (0.68)	1.11 (0.21)	1.65 (0.77)	<0.001
EcogSPVisspat	2.47 (0.85)	1.41 (0.54)	1.07 (0.19)	1.48 (0.69)	<0.001
EcogSPPlan	2.66 (0.90)	1.55 (0.68)	1.10 (0.32)	1.60 (0.81)	<0.001
EcogSPOrgan	2.90 (0.85)	1.63 (0.78)	1.12 (0.26)	1.68 (0.88)	<0.001
EcogSPDivatt	3.09 (0.84)	1.88 (0.79)	1.24 (0.46)	1.89 (0.93)	<0.001
EcogSPTotal	2.84 (0.62)	1.71 (0.61)	1.15 (0.22)	1.73 (0.75)	<0.001

129 The morphometry data set contains measures of cortical thickness (CT) and cortical
130 surface area (SA) for each of the thirty-four Desikan cortical surface ROIs in each hemisphere
131 processed using FreeSurfer (Desikan et al., 2006). Intra-cranial volume is also included as
132 a measure of cortical volume (CVol). The volumes of subcortical ROIs (both gray matter
133 and white matter regions/structures) are labelled as subcortical volumes (SVol). These

134 include 17 subcortical gray matter structures, 16 of which form eight hemispheric left-right
135 pairs. The unpaired subcortical gray matter ROI is the brainstem. There are 13 remaining
136 SVol measures which include the ventricles, cerebrospinal fluid (CSF), optic chiasm, corpus
137 callosum, and others. In total, 245 measures of brain morphometry are included.

138 **C.2 Scree plots for brain morphometry and cognition/behavior**

139 The scree plots in Figure S.1 show the total rank choices for cognition (left) and brain
140 morphometry (right) datasets. Dashed vertical lines correspond to the ‘elbow’ of the scree
141 plot (rank=5), the number of eigenvalues that account for at least 90% of total variability
142 (rank=9), and the number of eigenvalues accounting for at least 95% of total variation (rank
143 = 13).

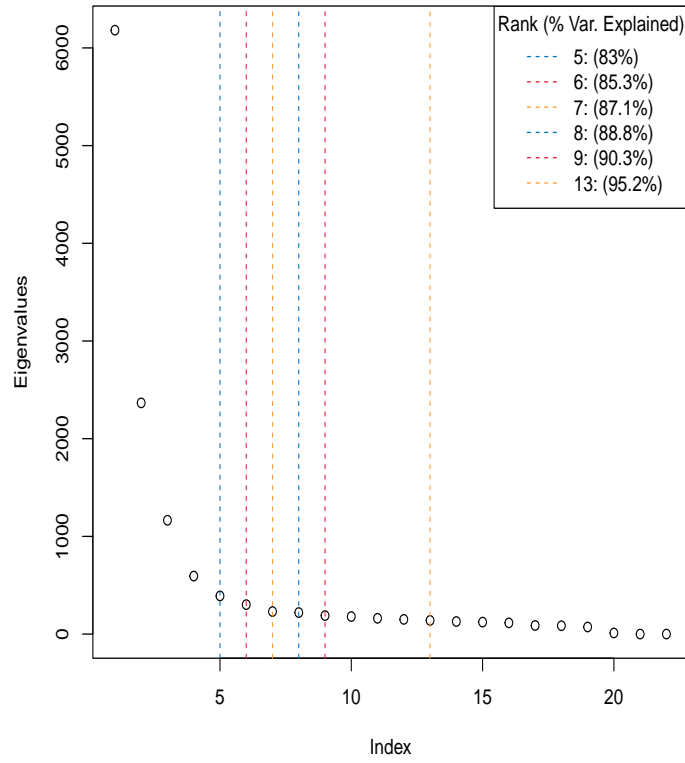
144 With brain morphometry, two values were proposed as the ‘elbow’ of the scree plot (rank
145 = 10 or 22). The other two ranks were chosen to account for at least 80% (rank = 53) and
146 at least 95% (rank = 113) of total variability. Figure S.1 shows the scree plot, each chosen
147 rank and the corresponding percentage of total variation.

148 In our analysis, we elected to use rank 5 for cognition and rank 10 for brain morphometry
149 based on our previous experience that choosing a lower rank can improve the selection of
150 the joint rank and also lead to a simpler, more interpretable decomposition.

151 **C.3 Individual subspaces**

152 Figures supporting the discussion of subject scores and variable loadings (Section 4.5 of the
153 main manuscript) from each dataset’s individual subspace are displayed in Figures S.2, S.3,
154 S.4, and S.5. Cognition loadings are discussed in the main manuscript. Brain loadings tend
155 to separate components by modality for some components; e.g., component 2 is dominated
156 by CT and component 4, by SVol measures. Other individual brain loading components com-
157 prise fewer ROIs with multiple modalities at several. For example component 5 is dominated
158 by SA and CVol in the same ROIs, including the insula and precentral gyrus.

Scree Plot of Cognition Measrues



Scree Plot of Brain Morphometry Measrues

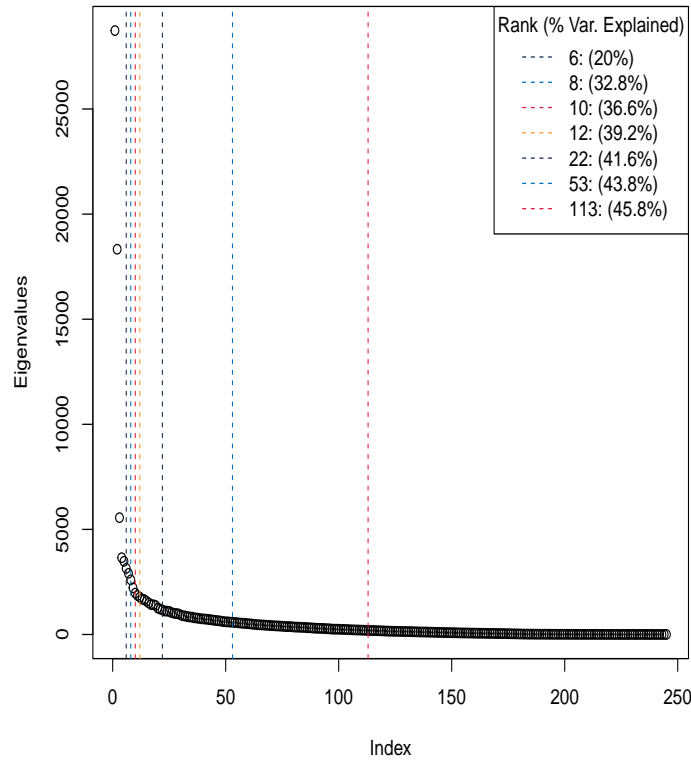


Figure S.1: Scree plots shows which values were chosen as total signal ranks. Choices depended the 'elbow' of the scree plot or by accounting for at least 80%, 90% ,or 95% of total variance.

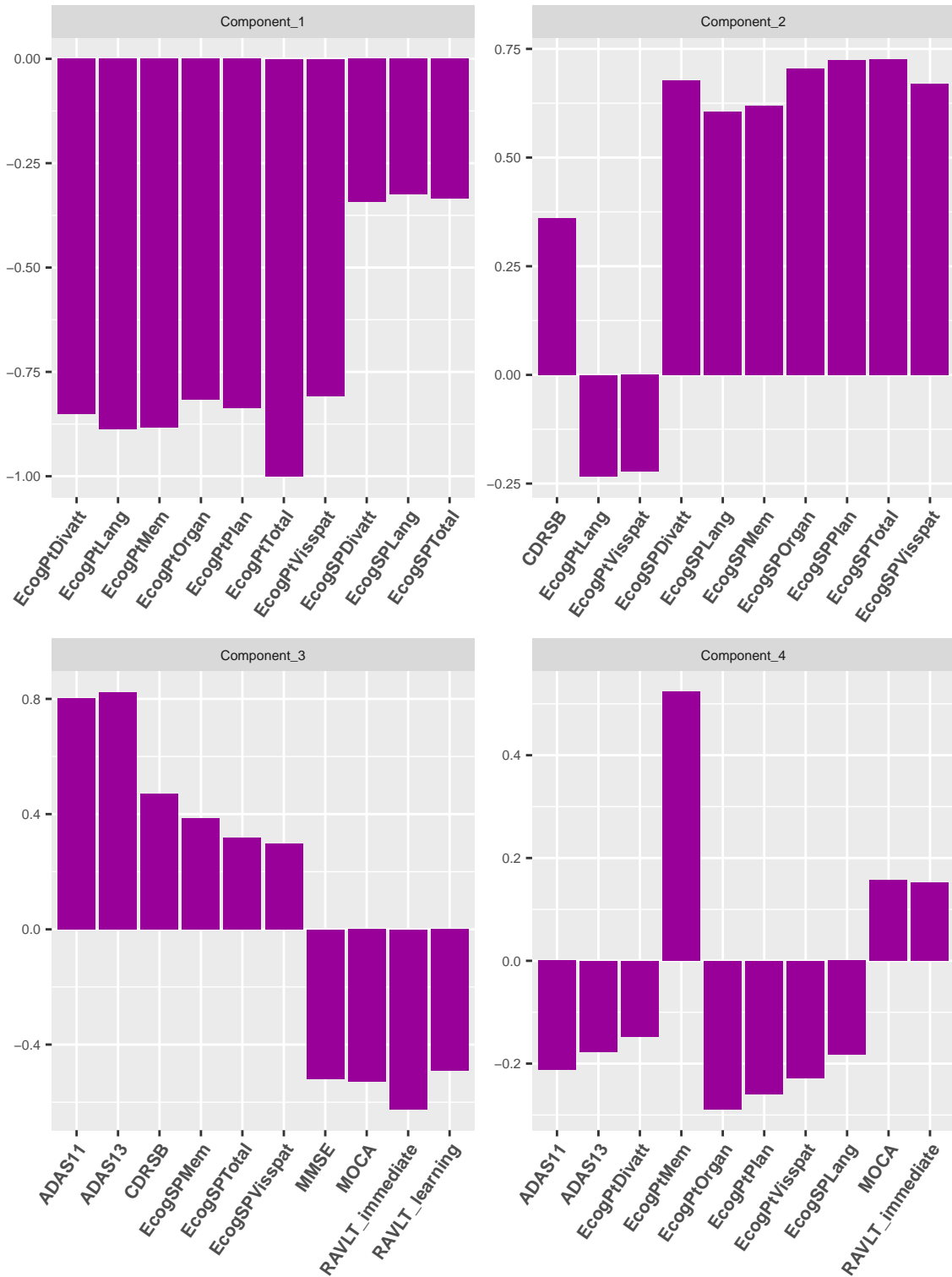


Figure S.2: 90th percentile of the absolute value of loadings onto each of the four components that compose the individual cognition subspace estimated via ProJIVE in the setting $K = 2$ (combining all brain morphometry measures as one dataset).

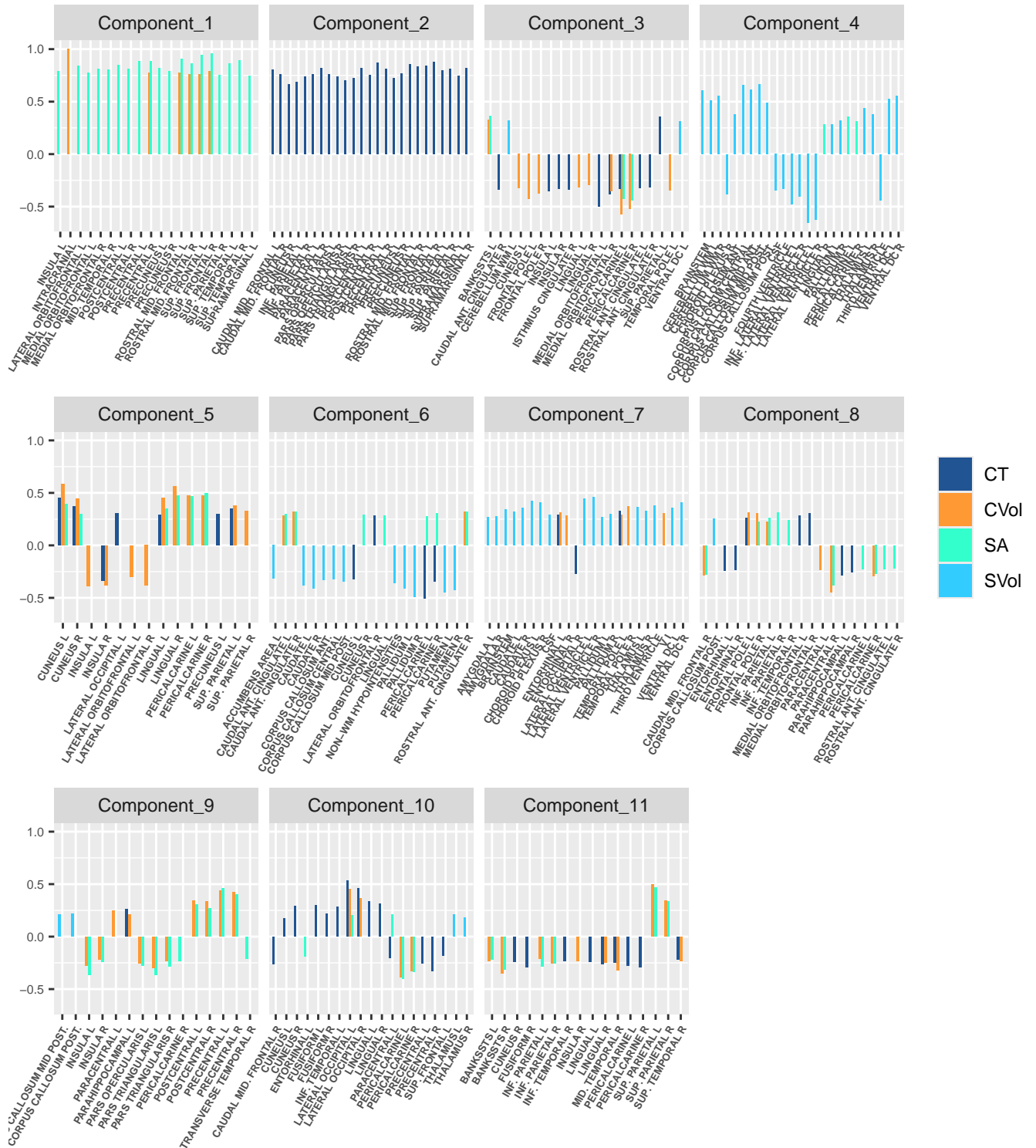


Figure S.3: 90th percentile of the absolute value of loadings onto each of the nine components that compose the individual morphometry subspace estimated via ProJIVE in the setting $K = 2$.

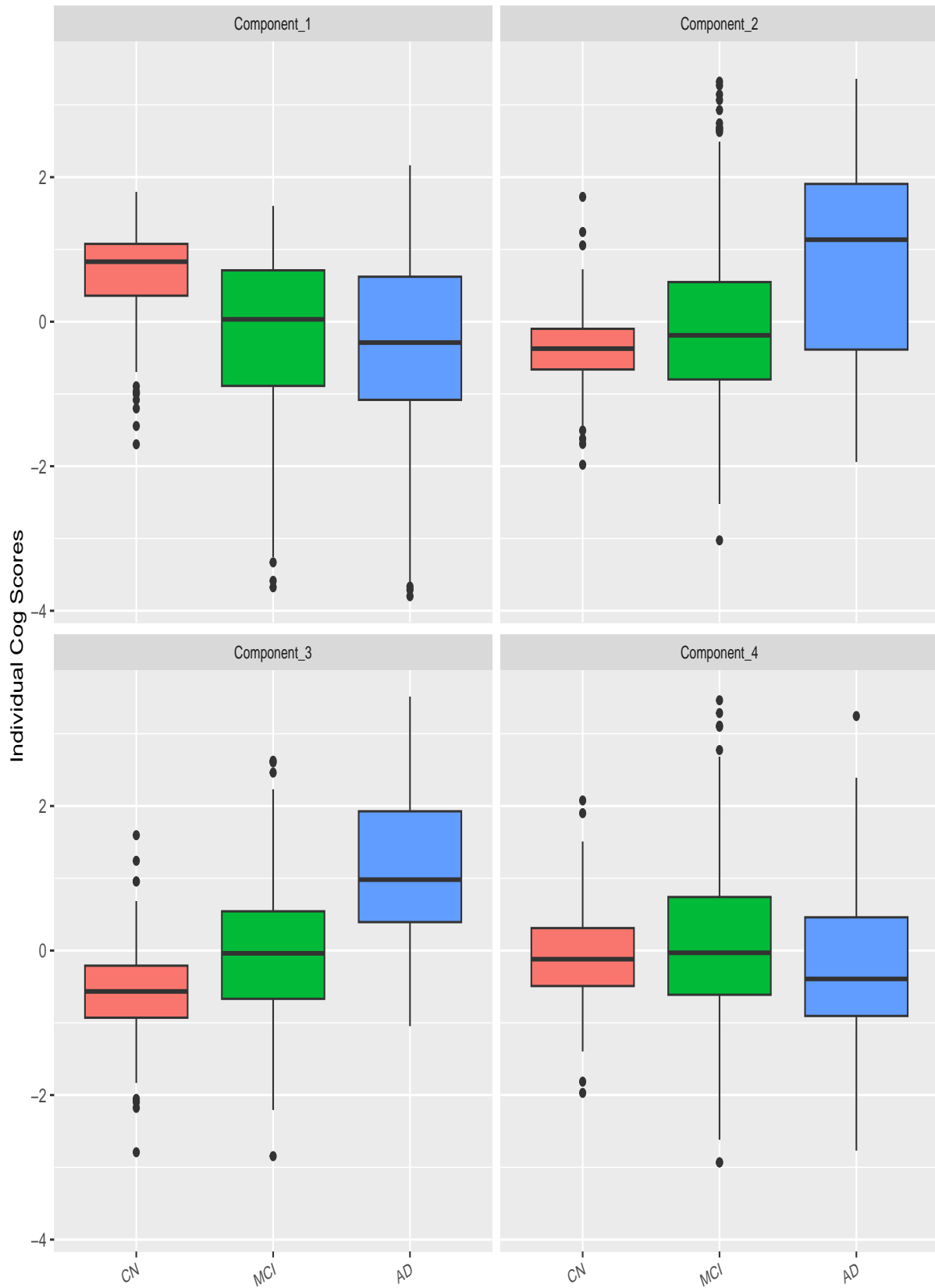


Figure S.4: Subject scores from each component of the individual cognition subspace estimated via ProJIVE in the setting $K = 2$.

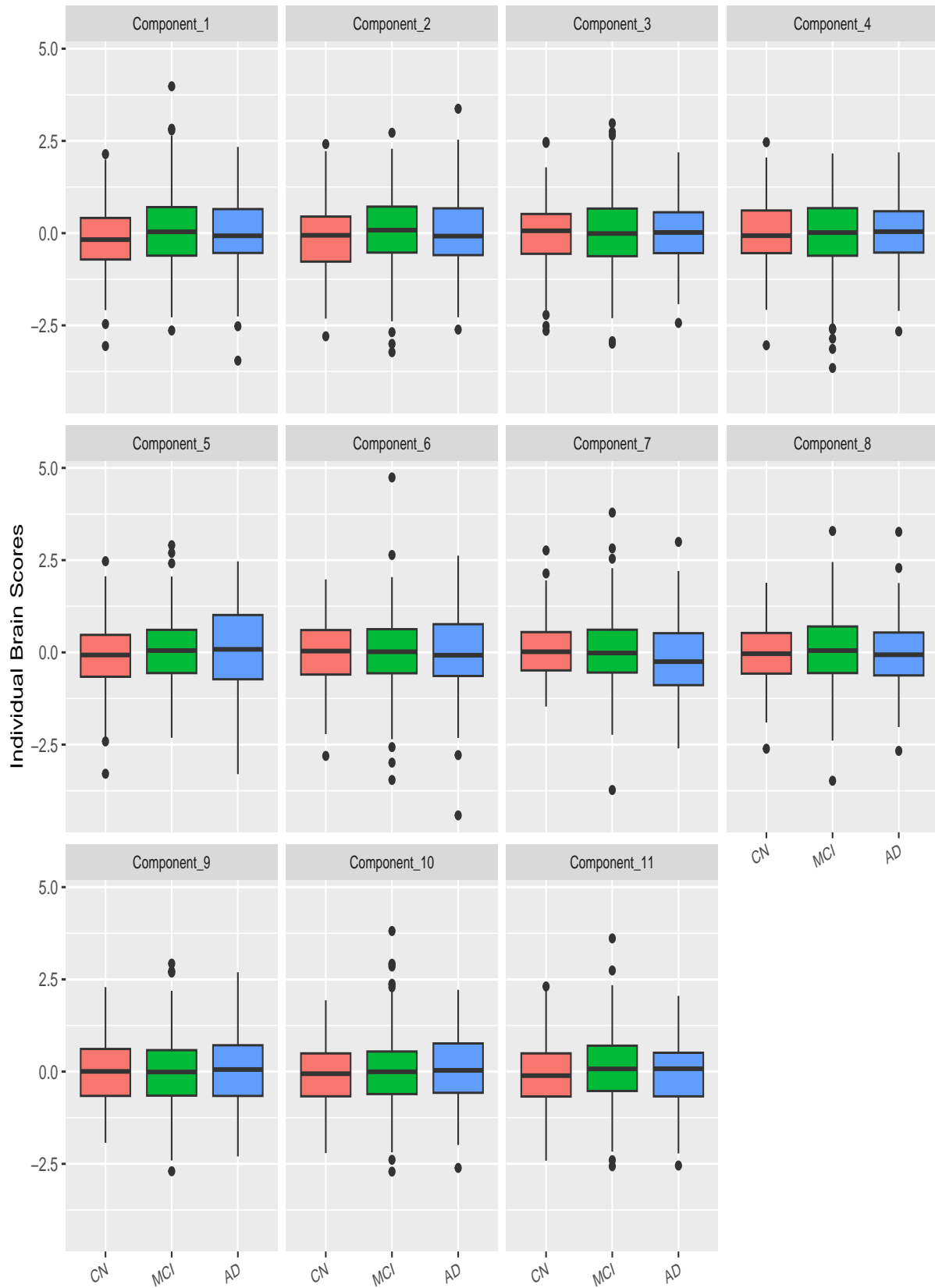


Figure S.5: Subject scores from each component of the individual brain morphometry subspace estimated via ProJIVE in the setting $K = 2$.

159 **D ProJIVE analysis of ADNI data with the specifica-** 160 **tion of $K = 5$ datasets**

161 The primary manuscript includes a brief review (Section 4.6) of ProJIVE as applied to the
162 same ADNI/TADPOLE data when each set of brain morphometry measures (CT, CVol, SA,
163 and SVol) were treated as separate datasets, resulting in a total of $K = 5$ data sets. To
164 complement this analysis, there is a brief discussion on choosing the features to comprise a
165 “dataset” (Section 5.)

166 **D.1 Joint Variable Loadings**

167 The top 10 variable loadings are displayed for cognition, and the top 15% of joint variable
168 loadings are displayed for cortical thickness, cortical volume, surface area, and subcortical
169 volume (Figure S.6). Notably, the distributions of the strongest variable loadings in the
170 $K = 5$ setting largely reflect findings from the $K = 2$ setting. In cognition, the only
171 difference in the pattern of these loadings is that EcogSPVisspat in the $K = 2$ setting is
172 replaced by the immediate-RAVLT score in the $K = 5$ setting. For morphometry measures,
173 a major difference lies in the presence of surface area (SA) loadings. However, recall that
174 loadings are scaled by their maximum absolute value for a dataset. Since the joint SA
175 loadings have a maximum absolute value of around 0.5, the strongest SA loadings are in the
176 individual SA subspace, as in the $K = 2$ case.

177 **D.2 Joint subject scores**

178 Joint subject scores from the $K = 5$ case show similar associations with exogenous variables
179 (i.e. PET biomarkers, diagnosis, and ApoE4) as in the $K = 2$ case (Figure S.7).

180 **D.3 Individual variable loadings**

181 Variable loadings onto the individual cognition subspace reflect somewhat divergent patterns
182 for analyses parameterized $K = 5$ (Figure S.8) and $K = 2$ (Figure S.4). Specifically, the

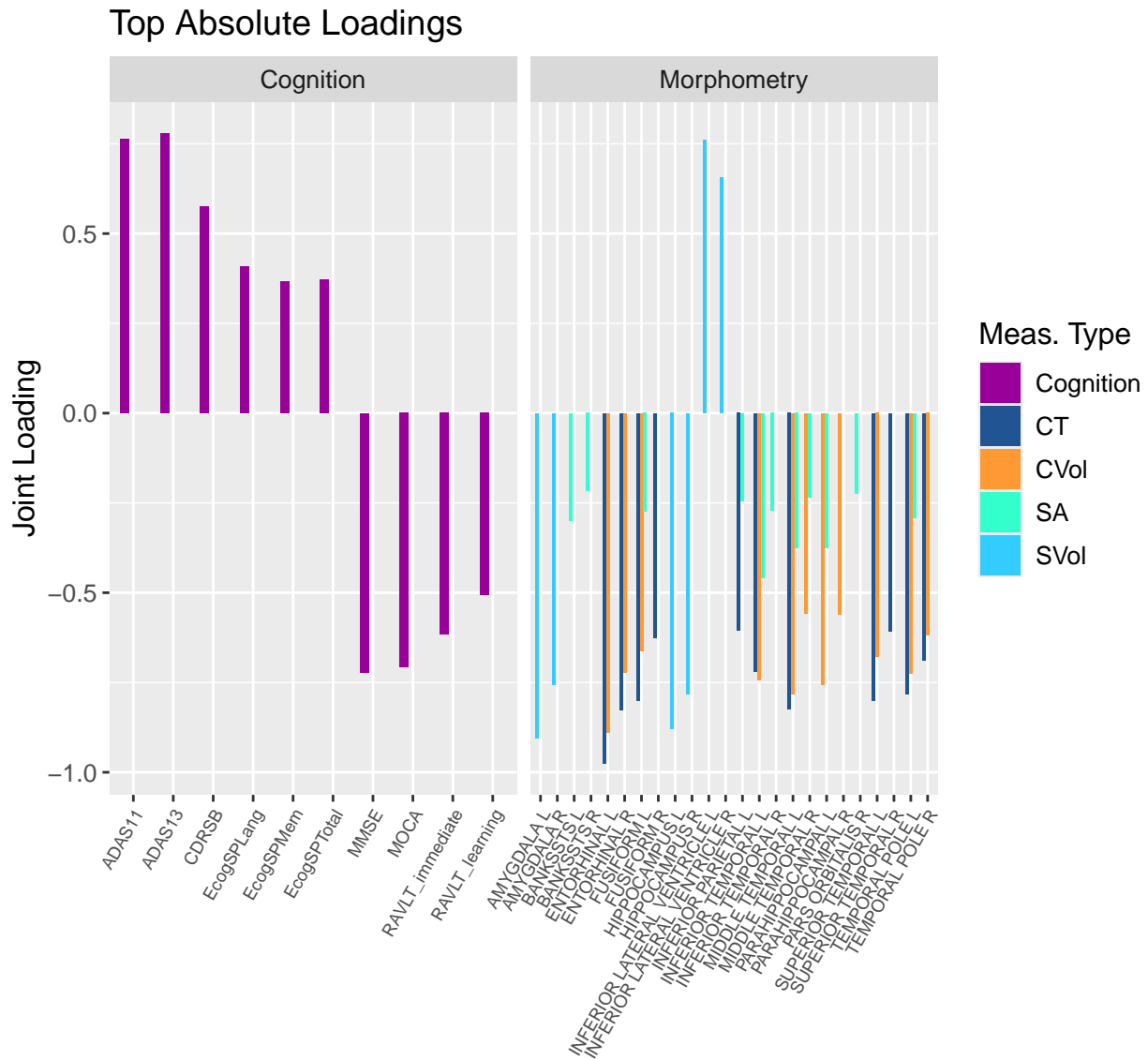


Figure S.6: Ten most extreme joint cognition loadings, six most extreme joint SVol loadings, and upper 85th percentile, respectively, of the absolute joint CT, CVol, and SA loadings estimated via ProJIVE in the setting $K = 5$ (treating each brain morphometry measure as a separate dataset).

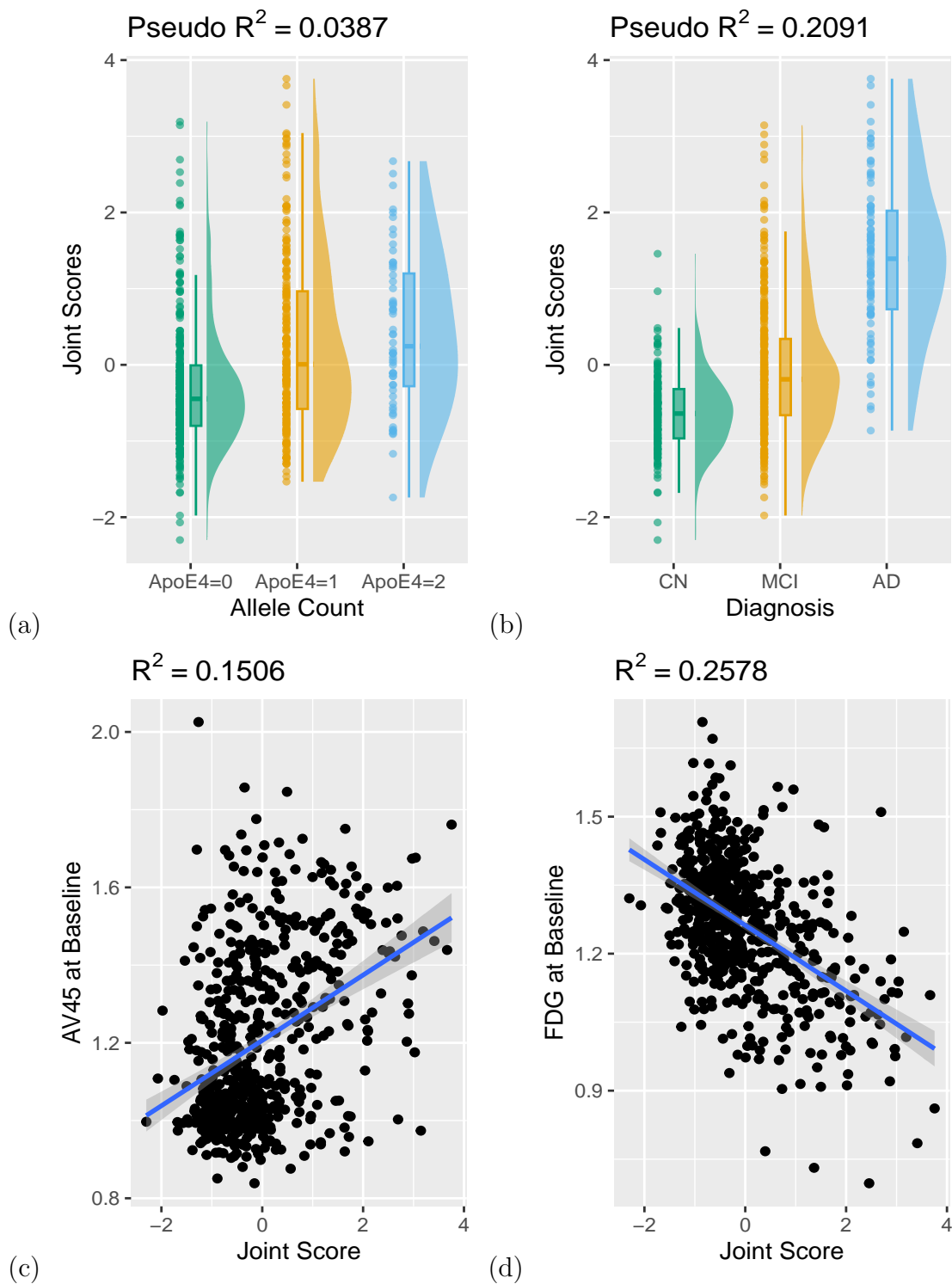


Figure S.7: Joint subject scores estimated via ProJIVE (for $K = 5$ in which brain morphometry data are separated into four different datasets) show separation by (a) the count of ApoE4 allele counts and (b) diagnosis via raincloud plots. (c) Scatterplot of joint subject scores and AV45 at Baseline with OLS regression line and confidence interval. (d) Scatterplot of joint subject scores and FDG at Baseline with OLS regression line and confidence interval. Results resemble findings from $K = 2$ in which all brain morphometry variables were combined into one dataset.

183 strongest loadings for components 1 and 2 are for the Everyday Cognition (Ecog) measures
184 in both settings. However, for $K = 5$, the study partner measures dominate component one
185 and patient measures dominate component 2, whereas the opposite holds for $K = 2$. In
186 component 3 of both analyses, the ADAS measures load in the opposite direction of MMSE,
187 MOCA, and RAVLT measures. However, for $K = 5$, RAVLT forgetting dominates compo-
188 nent 3, similar to component 4 of the $K = 2$ analyses. Lastly, component 4 loads strongly
189 onto the RAVLT-intermediate and -learning, MMSE, and MOCA measures in opposing the
190 direction to ADAS measures, similar to component 3 of the $K = 2$ results.

191 Comparing individual morphometry loadings across the two cases is not as straightfor-
192 ward since each set of morphometry measures has its subspace in the $K = 5$ case, and all
193 morphometry measures share an individual subspace in the $K = 2$ case. In the $K = 2$ case,
194 several components of the individual morphometry subspace appear to reflect a particular
195 type of morphometry measure. For instance, component 1 is dominated by SA measures,
196 component 2 by CT measures, and component 4 by SVol measures. However, the ROIs that
197 appear in component 1 do not dominate any component of the individual SA subspace found
198 in the $K = 5$ case, and similarly for CT and SVol. It is important to note that the individual
199 morphometry subspaces estimated in the $K = 2$ and $K = 5$ cases represent quite different
200 conceptualizations of the data. Therefore, divergence in their signals is to be expected. Each
201 set of individual morphometry loadings from the $K = 5$ case is displayed in Figure S.9.

202 **D.4 Individual subject scores**

203 As in the $K = 2$ case, all four individual cognition subject scores were associated with diag-
204 noses (section 4.5.2), with component one exhibiting the strongest association (McFadden’s
205 pseudo- $R^2 = 0.11$). Components one and four were associated with location shifts between
206 all three diagnoses (CN, MCI, and AD), while component two was associated with MCI and
207 component three with AD. Furthermore, pseudo- R^2 was much higher for component three
208 (≈ 0.04) than the same values for components three (≈ 0.02) and four (≈ 0.01 .) Associations
209 between ApoE4 counts and individual cognition scores were strongest for components one
210 and four. However, both were far weaker, each with pseudo- $R^2 = 0.01$, than the third com-

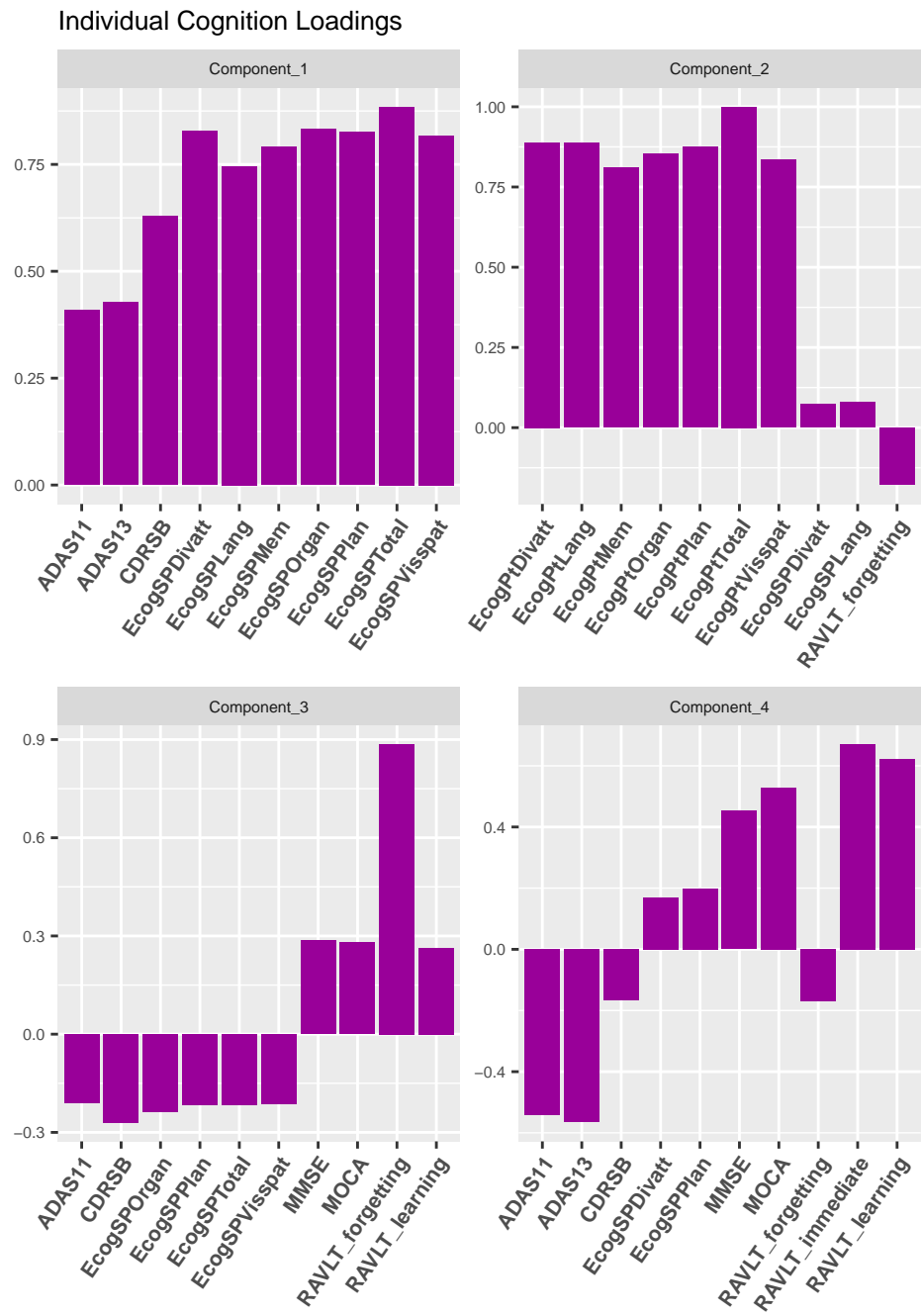


Figure S.8: subject scores individual cognition subspace estimated via ProJIVE in the setting $K = 5$.

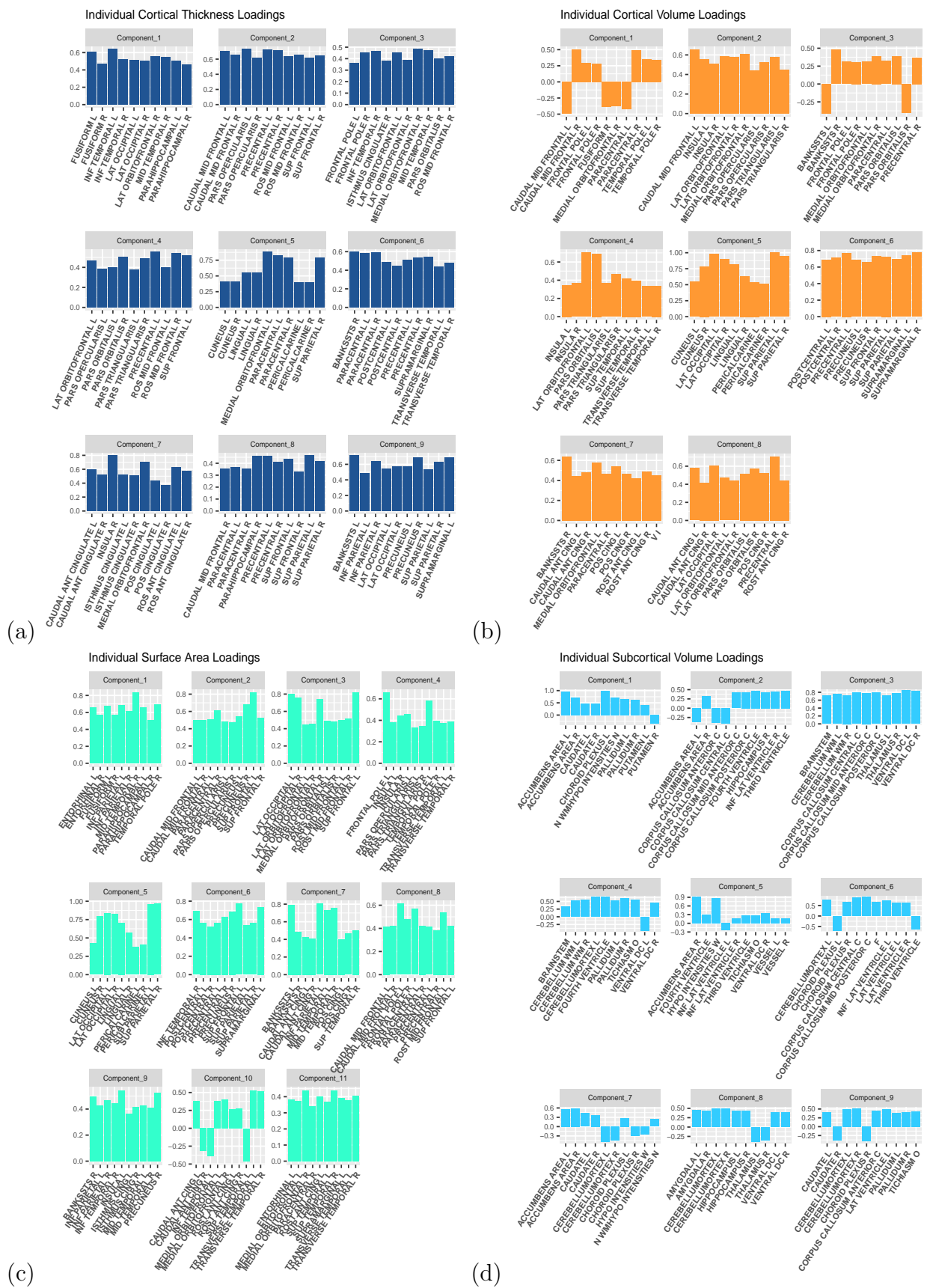


Figure S.9: Variable loadings for the individual brain morphometry subspaces estimated via ProJIVE in the setting $K = 5$. (a) CT, (b) CVol, (c) SA, (d) SVol.

211 ponent in the $K = 2$ case. As for the PET biomarkers, component 1 most strongly associated
212 with AV45 ($R^2 = 0.06$) and component 2 with FDG ($R^2 = 0.04$)

213 As in the main analysis of $K = 2$ datasets, we found no significant associations between
214 individual brain morphometry subject scores and diagnosis or ApoE4 allele counts. Individ-
215 ual subject scores from cortical thickness were associated with AV45 ($R^2 = 0.02$) and FDG
216 ($R^2 = 0.06$), especially component 9. Cortical volume scores were associated with FDG
217 ($R^2 = 0.02$). Surface area scores were not associated with any exogenous variables. Subcor-
218 tical volume scores were associated with with FDG ($R^2 = 0.04$) and AV45 ($R^2 = 0.02$).

219 References

- 220 Browne, M. W. (1979). The maximum-likelihood solution in inter-battery factor analysis.
221 *British Journal of Mathematical and Statistical Psychology*, 32(1):75–86.
- 222 Desikan, R. S., Ségonne, F., Fischl, B., Quinn, B. T., Dickerson, B. C., Blacker, D., Buckner,
223 R. L., Dale, A. M., Maguire, R. P., Hyman, B. T., and others (2006). An automated
224 labeling system for subdividing the human cerebral cortex on MRI scans into gyral based
225 regions of interest. *Neuroimage*, 31(3):968–980.
- 226 Farias, S. T., Mungas, D., Reed, B. R., Cahn-Weiner, D., Jagust, W., Baynes, K., and
227 DeCarli, C. (2008). The measurement of everyday cognition (ecog): scale development
228 and psychometric properties. *Neuropsychology*, 22(4):531.
- 229 Folstein, M. F., Folstein, S. E., and McHugh, P. R. (1975). “mini-mental state”: a practical
230 method for grading the cognitive state of patients for the clinician. *Journal of psychiatric*
231 *research*, 12(3):189–198.
- 232 Morris, J. C. (1997). Clinical dementia rating: a reliable and valid diagnostic and staging
233 measure for dementia of the alzheimer type. *International psychogeriatrics*, 9(S1):173–176.
- 234 Nasreddine, Z. S., Phillips, N. A., Bédirian, V., Charbonneau, S., Whitehead, V., Collin, I.,
235 Cummings, J. L., and Chertkow, H. (2005). The montreal cognitive assessment, moca:
236 a brief screening tool for mild cognitive impairment. *Journal of the American Geriatrics*
237 *Society*, 53(4):695–699.
- 238 Rey, A. (1941). L’examen psychologique dans les cas d’encéphalopathie traumatique.(les
239 problems.). *Archives de psychologie*.
- 240 Rey, A. (1958). L’examen clinique en psychologie.
- 241 Rosen, W. G., Mohs, R. C., and Davis, K. L. (1984). A new rating scale for alzheimer’s
242 disease. *The American journal of psychiatry*.

243 Ye, K. and Lim, L.-h. (2014). Schubert varieties and distances between subspaces of different
244 dimensions. *SIAM Journal on Matrix Analysis and Applications*, 37(3):1176–1197.